Solving the Fully Coupled Heart and Torso Problems of ElectroCardiology with a 3D Discrete Duality Finite Volume Method

Yves Coudière, Charles Pierre, Rodolphe Turpault

SOLVING THE FULLY COUPLED HEART AND TORSO PROBLEMS OF ELECTROCARDIOLOGY WITH A 3D DISCRETE DUALITY FINITE VOLUME METHOD

YVES COUDIÈRE, CHARLES PIERRE, AND RODOPLPHE TURPAULT

Abstract. A new 3D finite volume formulation and discretization is presented to simulate the electrocardiograms. It allows for the full coupling relations between the heart and the torso to be computed. Additionally, realistic ionic models are used, with very stiff dynamics. Hence, thousands of iterations are needed, each of which requires to solve a large and sparse linear system. The system is proved to be well-posed. Numerical results are presented, that rely on the choice of a good preconditioning technique.

1. Introduction

Computer models of the electrical activity in the myocardium are increasingly popular : the heart's activity generates an electric field in the torso, and produces a surface potential map whose measurement is the well-known electrocardiogram (ECG). It gives a non-invasive representation of the cardiac electrical function.

The electrical activity on the torso was first demonstrated to be directly connected to the heart beat more than 100 years ago [33]. the heart's behavior was first suggested to be well represented by a time-dependent electrical dipole. Afterward, more complex models based on dipole representation have also been used among which the oblique dipole layer [6]. Currently, the heart's electrical behavior is modeled by a system of Partial Differential Equations (PDE) of Reaction-Diffusion type [17]. Only the recent improvement of computing capabilities allows 3D computations to be achieved on the heart.

Naturally, understanding in depth the formation of the ECG is a major challenge for scientists, with a great impact on potential clinical applications. Currently, moving dipoles provide a quite complete view of the ECG, and is a standard analysis tool for cardiologists. However,

Date: January 11, 2006.

Laboratoire de Mathématiques Jean Leray, Nantes University and CNRS - UMR 6629, France.

the current computing capabilities allow for a bi-domain model to be used in ECG simulations, hopefully providing a deeper insight in ECG patterns. As a matter of fact, the dipole vision of ECGs can be assimilated to a top-down modeling approach, while the bi-domain heart coupled to the torso is more-less a bottom-up approach, that could be enriched as our microscopic understanding of living tissue improves.

The bi-domain equations model the heart as a continuum, despite its discrete structure. We refer to [7] for a mathematical derivation of the bi-domain equations, and to [13, 17] for reviews on the bi-domain equations. The torso is usually modeled as a passive electrical medium. Several authors address the problem of computing solutions to the isolated bi-domain equations, see [4] for a recent review. Here, interface conditions between the heart and the torso must be provided. Although the conditions that we propose to use have been derived in [18, 19] from an homogenization process, their physiological relevance is still an open modeling problem; and many authors propose variants of this conditions [4, 21]. We point out that experimental evidence show that the electrical activity of the heart cannot be decoupled to its electrical environment [27]. However it might be an important point to further investigate, for which numerical simulation may help.

While the bi-domain equation provide a large scale model of the structure of the heart muscle, it furthermore needs a microscopic description for cardiac muscular-cells membrane, providing a large variety of macroscopic models, ranging from 2 to about 30 equations. As a matter of fact, the electrical activity of the cell can be modeled in terms of ionic exchanges through the cell membrane and inside the cells. In the 50's Hodgkin and Huxley [16] introduced a first such model. Due to the sophistication of experimental techniques, there are currently several ones, see [17] for reviews. Models of Luo-Rudy's type [23, 25, 24, 11, 30, 31] are the most up-to-date concerning the behavior of the cardiac cell membrane. They are basically systems of ordinary differential equations, with at most 27 unknowns and very stiff dynamics. Simplified phenomenological models [12, 28] are usually used for 3D computations, assuming that the complex physiological ones are computationally to expensive. Several Luo-Rudy's like models were used to study their practical impact on the computation.

In this paper, we propose a first approach to compute some ECGs using the bi-domain equations together with a realistic ionic model and the coupling relations from [19]. In particular, the continuity of the current fluxes through the membrane cannot be simply achieved with the previous techniques [5, 20, 22]. This is why a finite volume

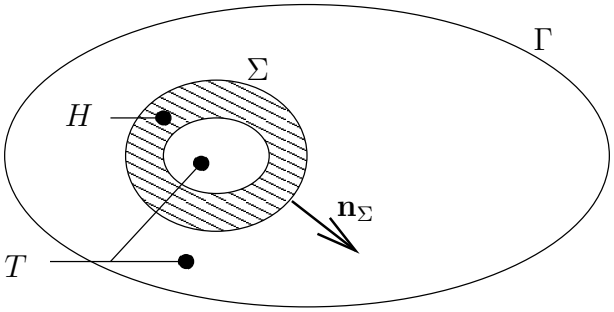

FIGURE 1. Heart and torso geometry

technique is used (see also [32]), that ensures the correct continuity relations. This is our main results for this problem.

Additionally, the numerical result depends on the construction of a new 3D finite volume technique that correctly accounts for anisotropy in the heart. It belongs to the family of Discrete Duality Finite Volume schemes (DDFV, [15, 9, 1]) and is basically a 3D extension of these techniques. We point out that the discrete problem is proved to be well-posed.

The problem involves solving accurately a large and ill-conditioned sparse linear problem at each time-step (meaning thousands of times), and preconditioning techniques are also investigated.

The paper is presented as follows. Section 2 recalls the principles of ECG computation using realistic ionic models, the bidomain model in the heart embedded in the torso. An insight to the meaning of finite volume methods is also presented. Section 3 introduces the meshes and many geometrical notations. Section 4 describes in details the finite volume method and its application to the bidomain problem. In section 4 and 5, the discrete problem is discussed (time-stepping for the ionic model and iterative method for the linear system), and computed ECGs are presented.

2. Principles of the computation of ECGs

The geometry and notations are described in figure 1: the heart and torso domain is an open and connected subset of $\mathbb{R}^d$ $(d = 2, 3)$ denoted by Ω; the heart itself is an open subset of Ω denoted by H, while the torso is an open subset of Ω denoted by T, both such that $\overline{\Omega} = \overline{H} \cup \overline{T}$. The boundary of Ω is denoted by Γ and the heart-torso interface is denoted by $\Sigma = \overline{H} \cap \overline{T}$. The unit normal to Σ from H to T is $\mathbf{n}_\Sigma$, and Γ is splitted into Γ^1 and Γ^2.

u	transmembrane potential	$[mV]$
u_e	extracellular potential	$[mV]$
u_T	extracardiac potential	$[mV]$
C_m	membrane capacitance	$[\mu F.cm^{-2}]$
A_m	membrane aspect ratio	$[cm^{-1}]$
$G_{i,e,T}$	conductivities	$[mS.cm^{-1}]$
I_{ion}	ionic current	$[\mu A]$
I_{st}	stimulation current	$[\mu A]$
t	time variable	$[s]$
x	space variable	$[cm]$

TABLE 1. Nomenclature

2.1. **The bidomain model.** The bidomain model represents the heart tissue at a macroscopic scale as the superimposition of two media, the intra- and extracellular media, which are actually distinct at the microscopic scale and separated by the active cell membrane. An intra- and an extracellular electrical potential, namely u_i and u_e are therefore defined in that framework on the whole heart domain H; their difference, *the transmembrane potential* $u = u_i - u_e$ (defined at the microscopic level on the active cell membrane) is here also defined on the whole heart volume H. Additionally, the cell membrane has a capacitive behavior, and after homogenization, the current balance writes, in H:

$$A_m C_m \left(\partial_t u + I_{ion}\right) = -\operatorname{div}(G_e \nabla u_e), \tag{1}$$

where A_m is the cell membrane surface to volume ratio, C_m is the capacitance per unit area, I_{ion} is the current induced by some biochemical ionic processes described below, and G_e is the conductivity of the extracellular medium.

The quasistatic electrical equilibrium is written for u_T, u_e, u_i :

$$\operatorname{div}\left((G_i + G_e)\nabla u_e\right) = -\operatorname{div}\left(G_i \nabla u\right) \quad \text{in } H, \tag{2}$$

$$\operatorname{div}\left(G_T \nabla u_T\right) = 0 \quad \text{in } T. \tag{3}$$

And then, the unknowns are the three functions

$$\begin{aligned} u &: (t,x) \in [0,+\infty) \times H \mapsto u(t,x) \in \mathbb{R}, \\ u_e &: (t,x) \in [0,+\infty) \times H \mapsto u_e(t,x) \in \mathbb{R}, \\ u_T &: (t,x) \in [0,+\infty) \times T \mapsto u_T(t,x) \in \mathbb{R}, \end{aligned}$$

and the conductivities G_i, G_e, G_T are supposed to be matrix valued smooth functions respectively on $\overline{H}$, $\overline{H}$ and $\overline{T}$, and for all $\xi \in \mathbb{R}^d$,

$$\forall x \in \overline{H},\ G_{i,e}(x)\xi \cdot \xi \geq \alpha|\xi|^2, \quad \text{and } \forall x \in \overline{T},\ G_T(x)\xi \cdot \xi \geq \alpha|\xi|^2, \tag{4}$$

for a given $\alpha > 0$.

Isolated heart. In the isolated case, $T = \emptyset$ and the only unknowns are u and u_e. The model is ruled by the boundary conditions

$$G_i \nabla u_e \cdot \mathbf{n}_\Sigma = -G_i \nabla u \cdot \mathbf{n}_\Sigma, \tag{5}$$

$$G_e \nabla u_e \cdot \mathbf{n}_H = 0. \tag{6}$$

Equation (5) rewrites $G_i \nabla u_i \cdot \mathbf{n}_\Sigma = 0$ (from $u = u_i - u_e$), meaning that no current flows out of the intracellular medium, and similarly (6) means that no current flows out of the extracellular medium.

Heart coupled to the torso. In order to compute some ECGs, the torso must be considered non-empty. The natural boundary conditions on the torso are

$$G_T \nabla u_T \cdot \mathbf{n}_T = 0 \quad (x \in \Gamma^2) \quad u_T = 0 \quad (x \in \Gamma^1). \tag{7}$$

Some conditions have to be set on the interface Σ. We choose to write

$$G_i \nabla u_e \cdot \mathbf{n}_H = -G_i \nabla u \cdot \mathbf{n}_H, \tag{8}$$

$$G_e \nabla u_e \cdot \mathbf{n}_H = G_T \nabla u_T \cdot \mathbf{n}_H, \tag{9}$$

$$u_e = u_T. \tag{10}$$

Like above, the condition (8) reads $G_i \nabla u_i \cdot \mathbf{n}_\Sigma = 0$, meaning that no current flows out of the heart from the intracellular medium, as it as been shown by physiological data at the cellular scale, [27]. Now (9) and (10) just express that the interaction between the heart and the torso is achieved via the extracellular domain.

Though these coupling interface condition have effectively been derived at a macroscopic scale [19], they remain relatively unused in the literature of ECGs computation, except in the works of Lines [22, 20], because they lead to technical and theoretical difficulties that we point out below. Also, these conditions deserve further investigations on a modeling point of view, [4].

Initial data. An initial data is provided on u only, since u_e is ruled by equation(2):

$$\forall x \in H, \quad u(0, x) = u_0(x). \tag{11}$$

A tentative variational formulation. It is a difficult task to solve the problem introduced in the previous subsection. In particular there has been no proof of the existence of solutions of the stationary problem : given the transmembrane potential $u : H \mapsto \mathbb{R}$, find $u_e : H \mapsto \mathbb{R}$

and $u_T : T \mapsto \mathbb{R}$, that satisfy (2), (3) and (8), (9), (10), and also (7). Nevertheless one can see that a simple variational technique fails to solve that problem.

Given u, an easy computation shows that any solution u_e, u_T of equations (2), (3) with the interface conditions (8)-(10) and the boundary conditions (7) defines a function on Ω,

$$v(x) = \begin{cases} u_e & \text{if } x \in H \\ u_T & \text{if } x \in T \end{cases} \tag{12}$$

verifying the weak problem

$$\forall \psi \in H^1(\Omega), \quad \int_\Omega G \nabla v \cdot \nabla \psi = -\int_H \operatorname{div}(G_e \nabla u)\psi, \tag{13}$$

where

$$G(x) = \begin{cases} G_i + G_e & \text{if } x \in H, \\ G_T & \text{if } x \in T. \end{cases} \tag{14}$$

The problem is that, conversely, any regular solution v of the weak problem (13) verifies (10) and (7), but not conditions (8) and (9). Instead, it verifies the interface condition

$$(G_i + G_e)\nabla u_e \cdot \mathbf{n}_H = G_T \nabla u_T \cdot \mathbf{n}_H. \tag{15}$$

With such a condition, the problem of finding u_e, u_T given u reduces to solving the variational equation (13), well suited to a finite element method.

Obtaining the solution with the interface conditions (8)-(10) within the finite element framework requires more work. Anyway, it has been computed ECGs with these interface conditions, [8, 5].

2.2. **The finite Volume Approach.** On the other hand, the finite volumes method consists in replacing the differential form of the equation by integral formulations on some *control volumes* (practically, the mesh cells). The three cases of control volumes inside the heart H, inside the torso T, and overlapping the interface Σ will be considered.

Assume that $V \subset \Omega$ is an arbitrary open subset of Ω with smooth boundary. A solution (u, u_e, u_T) of (1)-(7) verifies, for all $V \subset H$ (with $\mathbf{n}_V$ the unit normal outward of V)

$$A_m C_m \left(\frac{d}{dt} \int_V u + \int_V I_{ion} \right) = -\int_{\partial V} G_e \nabla u_e \cdot \mathbf{n}_V, \tag{16}$$

$$\int_{\partial V} (G_i + G_e)\nabla u_e \cdot \mathbf{n}_V = -\int_{\partial V} G_i \nabla u \cdot \mathbf{n}_V, \tag{17}$$

and for all $V \subset T$,

$$\int_{\partial V} G_T \nabla u_T \cdot \mathbf{n}_V = 0, \tag{18}$$

and at last for all V such that $V \cap H \neq \emptyset$ and $V \cap T \neq \emptyset$ (and the measure of $\Sigma \cap \partial V = 0$),

$$\int_{H\cap\partial V} (G_i + G_e)\nabla u_e \cdot \mathbf{n}_V + \int_{T\cap\partial V} G_T \nabla u_T \cdot \mathbf{n}_V = -\int_{H\cap\partial V} G_i \nabla u \cdot \mathbf{n}_V. \tag{19}$$

The interface conditions are taken into account in (19). Now, taken it into account also in (17), equations (17)-(19) can be rewritten in terms of v and G (defined in (12) and (14)):

$$\forall V \subset \Omega, \quad \int_{\partial V} G\nabla v \cdot \mathbf{n}_V + \int_{\Sigma\cap\partial V} G_e \nabla u_e \cdot \mathbf{n}_\Sigma = -\int_{H\cap\partial V} G_i \nabla u \cdot \mathbf{n}_V. \tag{20}$$

Conversely, any solution of (16) and (20) shall verify

- the three PDE (1), (2), (3) – just choose $V = B(x, \varepsilon)$ for $x \in H$ or $x \in T$ with $\varepsilon \to 0$;
- the interface condition (8) – choose $V = H \cap B(x, \varepsilon)$ for $x \in \Sigma$ and $\varepsilon \to 0$, and use the equations (2), (3);
- the interface condition (9) – choose $V = B(x, \varepsilon)$ for $x \in \Sigma$ and $\varepsilon \to 0$, and use the equations (2), (3) and the first interface condition.

Given a finite volume mesh, the problem is discretized in space using the integral equations (17) and (20), and resume to: find vector-valued functions[1]

$$u : t \in [0, +\infty) \mapsto u(t) \in \mathbb{R}^{N_T},$$
$$v : t \in [0, +\infty) \mapsto v(t) \in \mathbb{R}^{N},$$

such that for all $t \geq 0$,

$$A_m C_m \left(\dot{u}(t) + I_{ion}\right) = -A_e v(t), \tag{21}$$

$$Av(t) = -A_i u(t), \tag{22}$$

together with a discrete initial data on u,

$$u(0) = u^0 \in \mathbb{R}^{N_H}.$$

The matrices A_e, A and B are obtained from the integral form (16) and (20), and the boundary conditions (7).

As a matter of fact, this procedure splits the discrete problem into

- a *space problem* with unknowns u_e, u_T and data u, given by equation (22)

[1] N_H and N are, respectively, the number of unknowns in H and $\Omega = H \cup T$.

- an *evolution problem*, given by equation (21).

2.3. **Ionic current.** The ionic current I_{ion} which appears in (1) represents the current generated by the movement of ions through the cell membrane. The membrane itself is not permeable to ions therefore their migration inside or outside the cell is due to several processes.

Proteins inside the membrane allow specific ions to pass. These channels are numerous and characteristic of the cell-type. The ionic current of an ion X through the channel p is given by Ohm's law:

$$i_{X,p} = g_{X,p}(u - E_X). \tag{23}$$

where E_X is the equilibrium potential given by Nernst's law:

$$E_X = \frac{RT}{F} ln\Big(\frac{[X]_e}{[X]_i}\Big), \tag{24}$$

and $g_{X,p}$ is the conductivity. Channels may involve complex behavior and only allow a given ion to pass under particular conditions. The conductivity may therefore be written: $g_{X,p} = \overline{g_{X,p}} f(u, [X], \dots)$, where $\overline{g_{X,p}}$ is the maximum conductivity and f a function that ranges from 0 (closed) to 1 (open). As an example, the fast-$Na+$ current is:

$$i_{Na} = g_{Na}(u - E_{Na}). \tag{25}$$

The conductivity can be expressed with an Hodgkin-Huxley [16] formalism as $g_{Na} = \overline{g_{Na}} m^3 hj$ where m, h and j are activation or inactivation gates ruled by ordinary differential equations (ODE) e.g.:

$$d_t h = \alpha_h(1 - h) - \beta_h h \tag{26}$$

α_h and β_h are physiological parameters which may depend of various variables (u, concentrations, t,...). As a result the value of I_{ion}, which is the sum of all ionic currents through the membrane, depends on the resolution of several non-trivial ODE. Depending of the model, the number of these equations varies from 3 to a few dozen.

Complex models also involve pumps, exchangers and buffers in order to have a more realistic behavior, for example in the determination of the intracellular calcium concentration which is directly responsible of the muscular contraction.

At last, the ionic current appears as a function

$$I_{ion} = I_{ion}(t, u, [X]_i, [X]_e, \mathbf{w}),$$

where $[X]_{i,e}$ are the intra- and extracellular concentrations of ions X (Na, K, Ca) and $\mathbf{w}$ is a vector collecting the gate variables.

Initial data. Initial data are provided for the concentration $[X]_{i,e}$ and the gate variables $\mathbf{w}$.

For more information it is recommended to refer to the huge literature on the subject. Specifically, the reader is referred to [2], [23], [25], [24], [34], [30], [11] and [31] that describe the models implemented in our code.

3. Meshes and the Approximate Function Space

Remark 3.1. *The method is described on meshes which cells are triangles (2D) or tetraedra (3D), that are currently used on complex 2D/3D geometries. But hanging nodes are allowed, meaning that locally refined meshes and domain decomposition meshes are allowed.*

The 3D finite volume method requires to approximate the fluxes $G\nabla u \cdot \mathbf{n}$ of a piecewise constant function, which is still a challenge. Basically, an affine function is reconstructed from the piecewise constant one. The high complexity of 3D unstructured meshes requires complex notations. Therefore, the terminology from computational geometry (see [3]) is employed, and in particular, the notions of l-simplexes and l-faces of a simplex. We recall that l-simplexes are convex hulls of $l+1$ independent vertexes, so that they are nodes, edges, triangles (and tetraedra if $d = 3$), respectively for $l = 0, 1, 2$ (and 3 if $d = 3$).

Hereafter, $|X|$ denotes the l-dimensional measure of the l-dimensional polytope X.

3.1. **Meshes.** Consider a polyhedral bounded connected open subset Ω of $\mathbb{R}^d$ ($d = 2, 3$), and let Γ denote its boundary $\partial\Omega$. A mesh $\mathcal{M}$ is a collection of l-simplexes ($0 \leq l \leq d$) such that

(1) any face of a simplex in $\mathcal{M}$ is also a simplex in $\mathcal{M}$, and any l-simplex in $\mathcal{M}$ ($l < d$) is a face of a simplex in $\mathcal{M}$,
(2) $\cup_{K\in\mathcal{M}} K = \overline{\Omega}$,
(3) two simplexes K and L in $\mathcal{M}$ either do not intersect, or their intersection $\sigma = K \cap L$ is a l-simplex ($0 \leq l < d$) in $\mathcal{M}$ (ie that is a l-face of K or L). In this case, K and L are said to be *adjacent*. The $(d-1)$-faces that are intersections of two adjacent cells are called *interfaces*.

Conditions (1) and (2) ensure that $\overline{\Omega}$ is exactly the reunion of the d-simplexes (triangles/tetraedra) in $\mathcal{M}$, and that $\mathcal{M}$ is the collection of these d-simplexes and of exactly all their l-faces ($0 \leq l < d$, meaning, nodes, edges, facets). Condition (3) is usually replaced by

(3') two simplexes in $\mathcal{M}$ either do not intersect, or their intersection is a l-simplex ($0 \leq l < d$) that is their *common* l-face,

meaning that there is no hanging node in the mesh. A l-simplex ($0 \leq l < d$) intersection of two d-simplexes, $\sigma = K \cap L \in \mathcal{M}$, is necessarily a l-face of K or L from condition (1); but not necessarily of both K and L as in (3'). This is how hanging nodes are allowed.

Suppose for instance that $\sigma = K \cap L$ is a l-face of L, but not of K. Then there must exists $L_1, \dots L_p \in \mathcal{M}$ d-simplexes such that the l-face of K that contains σ is exactly $\cup_{i=1}^{p} K \cap L_i$: several L_i are needed to cover one l-face of K. Note that this l-face of K belongs to $\mathcal{M}$ although not needed (it is not an interface, as defined above).

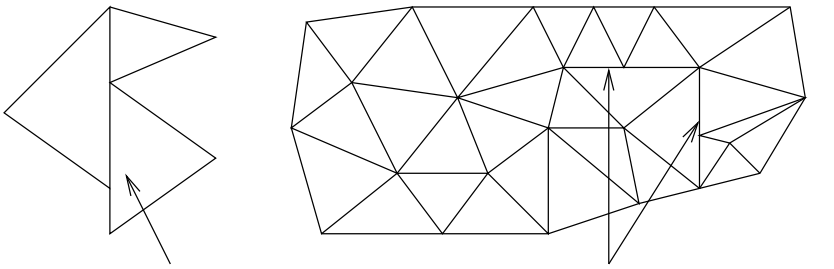

FIGURE 2. Meshes

The 0-faces in $\mathcal{M}$ are called *vertexes* and gathered into the set $\mathcal{V}$, the d-simplexes in $\mathcal{M}$ are called *cells* and gathered into the set $\mathcal{T}$, the $(d-1)$-faces in $\mathcal{M}$ are called *facets*; and facets that are intersections of two adjacent cells (ie interfaces) are gathered into the set $\mathcal{S}_\star$. The facets $\sigma \subset \Gamma$ are gathered into $\delta\mathcal{S}$, and we set $\mathcal{S} = \mathcal{S}_\star \cup \delta\mathcal{S}$. Obviously, $\delta\mathcal{S} \cap \mathcal{S}_\star = \emptyset$. The notations $N_\mathcal{T}, N_\mathcal{V}$ are used for the number of cells and of vertexes in $\mathcal{M}$. The following additional notations are required:

(1) for any $K \in \mathcal{T}$, x_K is the center of gravity of K, and for any $\sigma \in \mathcal{S}$, x_σ is the center of gravity of σ,
(2) for any $K \in \mathcal{T}$, δK denotes the subset of $\mathcal{S}$ such that $\partial K = \cup_{\delta K} \sigma$, and then $\delta K = \{\sigma \in \mathcal{S},\ \sigma \subset \delta K\}$,
(3) for any $A \in \mathcal{V}$, $\mathcal{S}_A$ denotes the subset of $\mathcal{S}$ of the faces for which A is a vertex, $\mathcal{S}_A = \{\sigma \in \mathcal{S},\ A \in \sigma\}$,
(4) for any $\sigma \in \mathcal{S}$, $\mathcal{V}_\sigma$ denotes the subset of $\mathcal{V}$ of the vertexes of σ, $\mathcal{V}_\sigma = \{A \in \mathcal{V},\ A \in \sigma\}$.

3.2. **V-cells and D-cells.** Summations over stencils of cells and stencils of faces are needed to formulate our scheme. New cells are associated to theses stencils (see figure 3:

(1) D-cells (for Diamond-cells) around the faces are constructed for $\sigma \in \mathcal{S}$,

(2) V-cells (for Vertex-cells) around the vertexes $A \in \mathcal{V}$ are constructed using S_A.

Hereafter, the notation conv$(\cdot)$ shall refer to the convex hull of a set of points in $\mathbb{R}^d$.

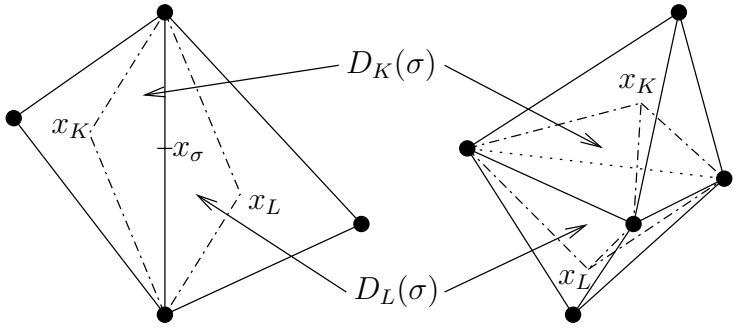

(a) D-cell in 2D (left) and 3D (right)

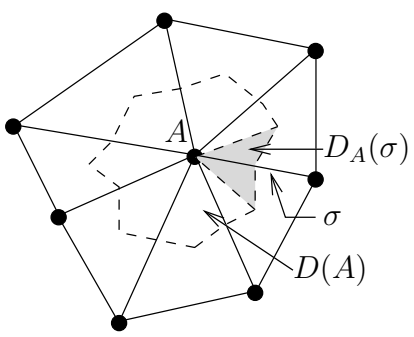

(b) Interior V-cell $D(A)$ in 2D

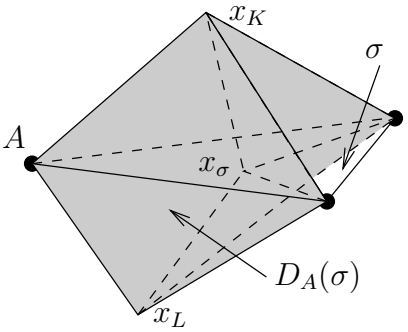

(c) Interior part $D_\sigma(A)$ of a V-cell in 3D

FIGURE 3. D-cells and V-cells

The D-cells. They are defined by

$$\forall \sigma = K \cap L \in \mathcal{S}_\star, \quad D(\sigma) = \text{conv}(\sigma \cup \{x_K\}) \cup \text{conv}(\sigma \cup \{x_L\}),$$
$$\forall \sigma = K \cap \Gamma \in \delta\mathcal{S}, \quad D(\sigma) = \text{conv}(\sigma \cup \{x_K\}).$$

We shall also use the notation $D_K(\sigma) = \text{conv}(\sigma \cup \{x_K\})$.

The V-cells. They are defined in two steps. First, for any $A \in \mathcal{V}$ and $\sigma \in \mathcal{S}_A$, define $D_A(\sigma) = \text{conv}(\{A, x_K, x_\sigma\}) \cup \text{conv}(\{A, x_L, x_\sigma\})$ if $d = 2$ and $\sigma = K \cap L \in \mathcal{S}_\star$, $D_A(\sigma) = \text{conv}(\{A, x_K, x_\sigma\})$ if $d = 2$ and $\sigma = K \cap \Gamma \in \delta\mathcal{S}$; and $D_A(\sigma) = \text{conv}(\{A, C, x_K, x_\sigma\}) \cup \text{conv}(\{A, C, x_L, x_\sigma\}) \cup$

$\mathrm{conv}(\{A,B,x_K,x_\sigma\}) \cup \mathrm{conv}(\{A,B,x_L,x_\sigma\})$ if $d=3$ and $\sigma = K\cap L = ABC \in \mathcal{S}_\star$, $D_A(\sigma) = \mathrm{conv}(\{A,C,x_K,x_\sigma\}) \cup \mathrm{conv}(\{A,B,x_K,x_\sigma\})$ if $d=3$ and $\sigma = K\cap\Gamma = ABC \in \delta\mathcal{S}$. Then the V-cells are defined by

$$\forall A \in \mathcal{V}, \quad D(A) = \cup_{\sigma\in\mathcal{S}_A} D_A(\sigma).$$

Note that the interiors of two different D-cells do not intersect, while $\overline{\Omega} = \cup_{\mathcal{S}} D(\sigma)$, so that $|\Omega| = \sum_{\mathcal{S}} |D(\sigma)|$.

The V-cells verify a similar property if $d=2$ (it is easy to check), but not if $d=3$. But the $D_A(\sigma)$ are not overlapping each other, and we have

$$\sum_{A\in\mathcal{V}} |D(A)| = \sum_{\sigma\in\mathcal{S}} \sum_{A\in\mathcal{V}_\sigma} |D_A(\sigma)|,$$

and then $\sum_{A\in\mathcal{V}_\sigma} |D_A(\sigma)| = (d-1)|D(\sigma)|$, because of the definitions of the $D_A(\sigma)$ so that

$$\sum_{A\in\mathcal{V}} |D(A)| = (d-1)|\Omega|.$$

3.3. **Additional requirement for the heart-torso problem.** The mesh has to be compatible with the geometry: we suppose that there exists two subsets $\mathcal{M}_H$ and $\mathcal{M}_T$ of $\mathcal{M}$ such that

$$X \in \mathcal{M}_H \Leftrightarrow X \subset \overline{H}, \quad X \in \mathcal{M}_T \Leftrightarrow X \subset \overline{T},$$

and then, $\mathcal{M}_H$ and $\mathcal{M}_T$ are just two distinct finite volume meshes. Additionally, the notations

- $\mathcal{T}_H$ and $\mathcal{T}_T$ refer to the cells $K \subset \overline{H}$ and $K \subset \overline{T}$;
- $\mathcal{V}_H$, $\mathcal{V}_T$, $\mathcal{V}_\Sigma$, $\mathcal{V}_1$, $\mathcal{V}_2$ refer to the nodes A in H, T, Σ, Γ^1 and Γ^2;
- $\mathcal{S}_H$, $\mathcal{S}_T$ and $\mathcal{S}_\Sigma$ refer to the interfaces σ in H, T and Σ;
- $\delta\mathcal{S}_1$ and $\delta\mathcal{S}_2$ refer to the facets σ on Γ^1 and Γ^2.

Note that $(\mathcal{T}_H, T_T)$ is a partition of $\mathcal{T}$, $(\mathcal{V}_H, \mathcal{V}_T, \mathcal{V}_\Sigma, \mathcal{V}_1, \mathcal{V}_2)$ is a partition of $\mathcal{V}$, $(\mathcal{S}_H, \mathcal{S}_T, \mathcal{S}_\Sigma)$ is a partition of $\mathcal{S}_\star$ and $(\delta\mathcal{S}_1, \delta\mathcal{S}_2)$ is a partition of $\delta\mathcal{S}$. The approximations of u and v will naturally be defined respectively on the two meshes $\mathcal{M}_H$ (of H) and $\mathcal{M}$ (of Ω) .

Concerning the D-cells and V-cells, except for $\sigma \in \mathcal{S}_\Sigma$ or $A \in \mathcal{V}_\Sigma$, a D-cell/V-cell is a subset of either $\overline{H}$ or $\overline{T}$.

Now, if $\sigma \in \mathcal{S}_\Sigma$, then $\sigma = K\cap L$ with $K \in \mathcal{T}_H$ and $L \in \mathcal{T}_T$ for instance. There are two useful notions of D-cell: the one in $\mathcal{M}_H$ and the one in $\mathcal{M}$. The former is naturally $D_K(\sigma)$ while the latter is $D(\sigma)$ (and we have $D(\sigma) = D_K(\sigma) \cup D_L(\sigma)$).

And if $A \in \mathcal{V}_\Sigma$, there are two useful notions of D-cell: the one in $\mathcal{M}_H$ and the one in $\mathcal{M}$. The former is $D(A) \cap \overline{H}$, denoted by $D_H(A)$ and the latter is $D(A)$.

4. The 3D Cell & Vertex Finite Volume Method

4.1. **The principle of the Method.** It consists in approximating the integral equations (16) and (20) on some control volumes V.

A standard finite volume method would use the $K \in \mathcal{T}_H$ as control volumes for (16) (evolution equation of u) and the $K \in \mathcal{T}$ as control volumes for (20) (quasi-static equation for v). Hence, the unknown would be the $(u_K)_{K\in\mathcal{T}_H}$ and the $(v_K)_{K\in\mathcal{T}}$ solving

$$A_m C_m \left(u'_K(t) + I_{ion}\right) = -\sum_{\sigma\in\delta K} F^e_{K\sigma} \quad (K \in \mathcal{T}_H), \tag{27}$$

$$-\sum_{\sigma\in\delta K} F_{K\sigma} = \sum_{\sigma\in\delta K} F^i_{K\sigma} \quad (K \in \mathcal{T}), \tag{28}$$

where $F^e_{K\sigma}$ estimates the flux $G_e\nabla u_e \cdot \mathbf{n}_K$ out of K through σ; $F_{K\sigma}$ estimates the flux $(G_i + G_e)\nabla u_e \cdot \mathbf{n}_K$ out of K through σ if $\sigma \in \mathcal{S}_H$, the flux $G_e\nabla u_e \cdot \mathbf{n}_K$ if $\sigma \in \mathcal{S}_\Sigma$, and the flux $G_T\nabla u_T \cdot \mathbf{n}_K$ if $\sigma \in \mathcal{S}_T \cup \delta\mathcal{S}$; and $F^i_{K\sigma}$ estimates the flux $G_i\nabla u \cdot \mathbf{n}_K$ out of K through σ if $\sigma \in \mathcal{S}_H$ and $F^i_{K\sigma} = 0$ otherwise (see eq. (20)).

Among many available techniques to compute the discrete fluxes, we choose the one that consists in adding unknowns $(u_A)_{A\in\mathcal{V}_H\cup\mathcal{V}_\sigma}$ and $(v_A)_{A\in\mathcal{V}}$ and using both the cells and nodes values to construct an approximate value of ∇u or ∇v on each side of σ. Following the approach in [14, 15, 9, 1] the new unknowns are assumed to be mean values on the V-cells (also called *dual cells*) and to solve the integral equations (16) and (20) on the V-cells:

$$A_m C_m \left(u'_A(t) + I_{ion}\right) = -\sum_{\sigma\in\mathcal{S}_A} F^e_{A\sigma} \quad (A \in \mathcal{V}_H \cup \mathcal{V}_\Sigma), \tag{29}$$

$$-\sum_{\sigma\in\mathcal{S}_A} F_{A\sigma} = \sum_{\sigma\in\mathcal{S}_A} F^i_{A\sigma} \quad (A \in \mathcal{V}\backslash\mathcal{V}_1), \tag{30}$$

and like above, $F^e_{A\sigma}$ estimates the flux $G_e\nabla u_e \cdot \mathbf{n}_A$ out of $D(A)$ through $D(\sigma)\cap\partial D(A)$; $F_{A\sigma}$ estimates the flux $(G_i+G_e)\nabla u_e \cdot \mathbf{n}_A$ or $G_T\nabla u_T \cdot \mathbf{n}_A$ or a combination of both, depending on A being in $\mathcal{V}_H$, $\mathcal{V}_T \cup \mathcal{V}_2$ or $\mathcal{V}_\Sigma$; and $F^i_{A\sigma}$ estimates the flux $G_i\nabla u \cdot \mathbf{n}_A$ if $\sigma \in \mathcal{S}_H$ and $F^i_{K\sigma} = 0$ otherwise (see eq. (20)).

The values v_A for $A \in \mathcal{V}_1$ are set according to the Dirichlet boundary condition

$$\forall A \in \mathcal{V}_1, \quad v_A = 0. \tag{31}$$

4.2. **The Semi-Discrete Problem.** As a consequence, we define

- the unknown $\mathbf{u} = (u_K, u_A)$ for $K \in \mathcal{T}_H$ and $\mathcal{V} \in \mathcal{V}_H \cup \mathcal{V}_\Sigma$ defining the space $FV(H)$ of dimension $N^{\mathcal{T}}_H + N^{\mathcal{V}}_H + N^{\mathcal{V}}_\Sigma$,

- the unknown $\mathbf{v} = (v_K, v_A)$ for $K \in \mathcal{T}$ and $\mathcal{A} \in \mathcal{V}$, assuming that $v_A = 0$ if $A \in \mathcal{V}_1$, defining the space $FV(\Omega)$ of dimension $N^{\mathcal{T}} + N^{\mathcal{V}} - N_1^{\mathcal{V}}$,

where $N_H^{\mathcal{T}}$, $N_H^{\mathcal{V}}$, $N_\Sigma^{\mathcal{V}}$, $N^{\mathcal{T}}$, $N^{\mathcal{V}}$, $N_1^{\mathcal{V}}$ are respectively the number of elements in $\mathcal{T}_H$, $\mathcal{V}_H$, $\mathcal{V}_\Sigma$, $\mathcal{T}$, $\mathcal{V}$ and $\mathcal{V}_1$.

In the next section, we shall explain how to construct (linearly) some piecewise constant gradients $\mathbf{p}_{K\sigma}(\mathbf{u})$ and $\mathbf{p}_{K\sigma}(\mathbf{v})$ on each $D_K(\sigma)$, respectively for $K \in \mathcal{T}_H$ and $\sigma \in \delta K$ and for $K \in \mathcal{T}$ and $\sigma \in \delta K$.

The conductivities are approximated by $G_{i\sigma} = G_i(x_\sigma)$, $G_{e\sigma} = G_e(x_\sigma)$ and $G_{T\sigma} = G_T(x_\sigma)$.

As a consequence, using the $G_{i\sigma}$, $G_{e\sigma}$, $G_{T\sigma}$ and the $\mathbf{p}_{K\sigma}$ provides exactly a two square systems of $N_H^{\mathcal{T}} + N_H^{\mathcal{V}} + N_\Sigma^{\mathcal{V}}$ and $N^{\mathcal{T}} + N^{\mathcal{V}} - N_1^{\mathcal{V}}$ linear equations; Respectively

$$\begin{aligned} A_m C_m \left(\mathbf{u}'(t) + I_{ion}\right) &= -A_e \mathbf{v}(t) \quad \text{in } FV(H), \\ A\mathbf{v}(t) &= -A_i \mathbf{u}(t) \quad \text{in } FV(\Omega). \end{aligned}$$

4.3. **Estimates of the gradient.** In this section, we consider the general case of a conductivity matrix $G(x)$ defined on $\overline{\Omega}$ and a piecewise constant function $\mathbf{u} = (u_K, u_A)$ defined on a mesh $\mathcal{M}$ of Ω, and show how its gradient is calculated. It would apply both to $\mathbf{u} \in FV(H)$ on $\mathcal{M}_H$ and to $\mathbf{v} \in FV(\Omega)$ on $\mathcal{M}$.

There are enough data in each $D_K(\sigma)$, namely u_K and u_A for all $A \in \mathcal{V}_\sigma$, to construct a consistent approximation of $\nabla \mathbf{u}$. But since we also want to ensure a continuity condition on σ, auxiliary unknowns u_σ for the $\sigma \in \mathcal{S}$ are added and tuned in order to ensure the needed continuity conditions. Now, remark that $\mathrm{conv}(x_K, x_\sigma, A)$ $(A \in \mathcal{V}_\sigma)$ in 2D and $\mathrm{conv}(x_K, x_\sigma, A, B)$ $(A, B \in \mathcal{V}_\sigma,\ A \neq B)$ in 3D is a triangulation (2D) or a tetraedrisation (3D) of $D_K(\sigma)$, see figure 3. As a consequence, a simple P1-Lagrange procedure provides a function $\mathbf{u}^\star$ that interpolates $\mathbf{u}$ at x_K, x_σ and the x_A $(A \in \mathcal{V}_\sigma)$. The gradient $\mathbf{p}_{K\sigma}(\mathbf{u})$ is the mean gradient of $\mathbf{u}^\star$ on $D_K(\sigma)$,

$$\mathbf{p}_{K\sigma}(\mathbf{u}) = \frac{1}{|D_K(\sigma)|} \int_{D_K(\sigma)} \nabla \mathbf{u}^\star = \frac{1}{|D_K(\sigma)|} \int_{\partial D_K(\sigma)} \mathbf{u}^\star \mathbf{n}, \tag{32}$$

where $\mathbf{n}$ is the unit exterior normal to $D_K(\sigma)$, and $\mathbf{u}^\star$ is piecewise linear on the facets of $\partial D_K(\sigma)$ and given by its nodes values u_K, u_σ and u_A $(A \in \mathcal{V}_\sigma)$.

Proposition 4.1 (Expression of the gradient)**.** *The equations* (32) *uniquely define some gradients* $\mathbf{p}_{K\sigma}(\mathbf{u})$*, given by*

$$d\mathbf{p}_{K\sigma}(\mathbf{u})|D_K(\sigma)| = (u_\sigma - u_K) N_{K\sigma} - \sum_{A \in \mathcal{V}_\sigma} u_A N_{A\sigma}^K, \tag{33}$$

for $K \in \mathcal{T}$ and $\sigma \in \delta K$; Where in any case

$$N_{K\sigma} = \int_\sigma \mathbf{n}_K, \quad N^K_{A\sigma} = \int_{D_K(\sigma)\cap\partial D(A)} \mathbf{n}_A, \tag{34}$$

except if $\sigma \in \delta\mathcal{S}$, where

$$N^K_{A\sigma} = \int_{D_K(\sigma)\cap\partial D(A)} \mathbf{n}_A - \frac{d-1}{d} N_{K\sigma}. \tag{35}$$

Proof. We need now to introduce some notations to describe the boundary of $D_K(\sigma)$. Let $\mathcal{V}_\sigma = \{A_1, \dots A_d\}$ be the vertexes of σ oriented directly with respect to the direction $\mathbf{n}_{K\sigma}$ unit normal to σ outward of K; For $i = 1 \dots d$, let $\mathbf{n}_{iK}$ denote the unit normal to the facet

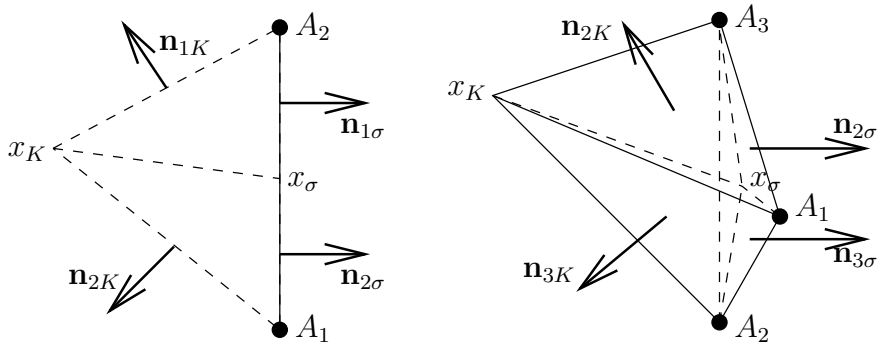

(a) 2D case (b) 3D case

FIGURE 4. normals to $D(\sigma)$

$F_{Ki} = \mathrm{conv}(\{x_K, x_j,\ j \neq i\})$ of $D_K(\sigma)$[2], pointing outward of $D_K(\sigma)$ (figure 4); let $F_{i\sigma} = \mathrm{conv}(\{x_\sigma, x_j,\ j \neq i\})$ be the other facets of $D_K(\sigma)$; and additionally,

$$N_{iK} = \int_{F_{Ki}} \mathbf{n}_{iK}.$$

Now, remark that the unit normal to $F_{i\sigma}$ outward of $D_K(\sigma)$ is just $\mathbf{n}_{K\sigma}$, and we can define

$$N_{i\sigma} = \int_{F_{i\sigma}} \mathbf{n}_{i\sigma} = \frac{1}{d} N_{K\sigma},$$

because x_σ is the center of gravity of σ. Of course, we have $\partial D_K(\sigma) = \cup_{i=1}^d F_{Ki} \cup F_{i\sigma}$. The function $\mathbf{u}^\star$ being linear on each of the facets F_{Ki},

[2]that means the facet opposite to A_i and its outward unit normal.

$F_{i\sigma}$, we find that

$$\begin{aligned}(36)\quad &\mathbf{p}_{K\sigma}(\mathbf{u})|D_K(\sigma)| \\ &= \sum_{i=1}^{d}\left(\frac{u_K+\sum_{j\neq i}u_{A_j}}{d}N_{iK}+\frac{u_\sigma+\sum_{j\neq i}u_{A_j}}{d}N_{i\sigma}\right) \\ &= \frac{u_K}{d}\sum_{i=1}^{d}N_{iK}+\frac{u_\sigma}{d}\sum_{i=1}^{d}N_{i\sigma}+\sum_{i=1}^{d}\frac{u_{A_i}}{d}\sum_{j\neq i}(N_{jK}+N_{j\sigma}).\end{aligned}$$

But we have

$$(37)\qquad \sum_{i=1}^{d}N_{i\sigma}=N_{K\sigma},\quad N_{K\sigma}+\sum_{i=1}^{d}N_{iK}=0,$$

because $\int_{D_K(\sigma)}\mathbf{n}=0$. Now we have $\int_V\mathbf{n}=0$ also for $V=D(A)\cap D_K(\sigma)$; And then if $\sigma\in\mathcal{S}_\star$,

$$(38)\qquad N^K_{A_i\sigma}=\int_{D(\sigma)\cap\partial D(A_i)}\mathbf{n}_{A_i}=-\sum_{j\neq i}(N_{jK}+N_{j\sigma}),$$

because $\sigma\not\subset\partial D(A_i)$. At last, if $\sigma\in\delta\mathcal{S}$, then we have

$$(39)\qquad \int_{D(\sigma)\cap\partial D(A_i)}\mathbf{n}_{A_i}=-\sum_{j\neq i}N_{jK},$$

because $\sigma\subset\partial D(A_i)$.

Using (37), (38) and (39) (note that $\sum_{j\neq i}N_{j\sigma}=\frac{d-1}{d}N_{K\sigma}$) in (36) ends the proof. □

Proposition 4.2 (Conservativity, continuous case)**.** *Suppose that G is continuous and u_σ is ruled by the conservativity relation (for $\sigma=K\cap L\in\mathcal{S}_\star$)*

$$G(x_\sigma)\mathbf{p}_{K\sigma}(\mathbf{u})\cdot N_{K\sigma}+G(x_\sigma)\mathbf{p}_{L\sigma}(\mathbf{u})\cdot N_{L\sigma}=0.$$

Then we have $\mathbf{p}_{K\sigma}=\mathbf{p}_{L\sigma}=\mathbf{p}_\sigma$, given by

$$(40)\qquad d\mathbf{p}_\sigma|D(\sigma)|=(u_L-u_K)N_{K\sigma}-\sum_{A\in\mathcal{V}_\sigma}u_AN_{A\sigma},$$

with $N_{A\sigma}=N^K_{A\sigma}+N^L_{A\sigma}$.

Proof. Due to the conservativity relation, $\mathbf{p}_{K\sigma}$ and $\mathbf{p}_{L\sigma}$ are the same in the direction $G(x_\sigma)\mathbf{n}_{K\sigma}$. Since $\mathbf{p}_{K\sigma}\cdot(x_A-x_B)=\mathbf{p}_{L\sigma}\cdot(x_A-x_B)=u_A-u_B$ for any $A,B\in\mathcal{V}_\sigma$, we have $\mathbf{p}_{K\sigma}=\mathbf{p}_{L\sigma}$ $(=\mathbf{p}_\sigma)$. Equation (40) is then an easy consequence of (33). □

Proposition 4.3 (Conservativity, discontinuous case)**.** *Suppose that the interface $\sigma = K \cap L \in \mathcal{S}_\star$ is a discontinuity surface for G, and it holds the limits $G_{K\sigma} = \lim_{0-} G(x_\sigma + t\mathbf{n}_{K\sigma})$ and $G_{L\sigma} = \lim_{0+} G(x_\sigma + t\mathbf{n}_{K\sigma})$. Then the value of u_σ is uniquely determined by*

$$u_\sigma \left(\frac{N_{K\sigma} G_{K\sigma} N_{K\sigma}}{|D_K(\sigma)|} + \frac{N_{L\sigma} G_{L\sigma} N_{L\sigma}}{|D_L(\sigma)|} \right) = u_K \frac{N_{K\sigma} G_{K\sigma} N_{K\sigma}}{|D_K(\sigma)|} + u_L \frac{N_{L\sigma} G_{L\sigma} N_{L\sigma}}{|D_L(\sigma)|} + \sum_{A \in \mathcal{V}_\sigma} u_A \left(\frac{N^K_{A\sigma} G_{K\sigma} N_{K\sigma}}{|D_K(\sigma)|} + \frac{N^L_{A\sigma} G_{L\sigma} N_{L\sigma}}{|D_L(\sigma)|} \right).$$

Proof. It is an easy consequence of the conservativity relation

$$G_{K\sigma} \mathbf{p}_{K\sigma}(\mathbf{u}) \cdot N_{K\sigma} + G_{L\sigma} \mathbf{p}_{L\sigma}(\mathbf{u}) \cdot N_{L\sigma} = 0. \tag{41}$$

□

4.4. **Boundary Conditions.** The auxiliary unknowns u_σ for $\sigma \in \delta\mathcal{S}$ are computed in order to account for the boundary conditions. Suppose that $\delta\mathcal{S}$ is splitted into $\delta\mathcal{S}^1$ and $\delta\mathcal{S}^2$ collecting the facets concerned respectively by the Dirichlet and the Neumann homogeneous conditions. Then we simply set

$$\forall \sigma \in \delta\mathcal{S}^1, \quad u_\sigma = 0; \tag{42}$$

and

$$\forall \sigma \in \delta\mathcal{S}^2, \quad G(x_\sigma) \mathbf{p}_{K\sigma}(\mathbf{u}) \cdot \mathbf{n}_{K\sigma} = 0, \tag{43}$$

so that

$$u_\sigma = u_K + \sum_{A \in \mathcal{V}_\sigma} u_A \frac{N^K_{A\sigma} G_{K\sigma} N_{K\sigma}}{N_{K\sigma} G_{K\sigma} N_{K\sigma}},$$

$$d|D_K(\sigma)| \mathbf{p}_{K\sigma} = \sum_{A \in \mathcal{V}_\sigma} u_A \left(\frac{N^K_{A\sigma} G_{K\sigma} N_{K\sigma}}{N_{K\sigma} G_{K\sigma} N_{K\sigma}} N_{K\sigma} - N^K_{A\sigma} \right).$$

4.5. **Properties of the Discrete Gradient.**

Proposition 4.4 (Solutions of $\mathbf{p}_{K\sigma} = 0$)**.** *Given $\mathbf{u} \in FV(\Omega)$ defined on a mesh $\mathcal{M}$ of Ω, and some values $(u_\sigma)_{\sigma \in \mathcal{S}}$, we have*

$$\mathbf{p}_{K\sigma} = 0, \ \forall K \in \mathcal{T}, \ \forall \sigma \in \delta K \ \Leftrightarrow \ \exists a, b \in \mathbb{R}, \quad u_\sigma = u_K = a \ (K \in \mathcal{T}, \sigma \in \delta K), \quad u_A = b \ (A \in \mathcal{V}). \tag{44}$$

Proof. For $K \in \mathcal{T}$ and $\sigma \in \delta K$, the family $(N_{A\sigma}^K)_{A\in\mathcal{V}_\sigma}$ has d vectors in $\mathbb{R}^d$ such that

$$\sum_{A\in\mathcal{V}_\sigma} N_{A\sigma}^K = \sum_{i=1}^{d}\sum_{j\neq i}(N_{Kj}+N_{j\sigma}) = (d-1)\sum_{j=1}^{d}(N_{Kj}+N_{j\sigma}) = (d-1)\int_{\partial D_K(\sigma)}\mathbf{n} = 0. \tag{45}$$

Hence, the rank of $(N_{A\sigma}^K)_{A\in\mathcal{V}_\sigma}$ is $d-1$, and additionally (for $\sigma \in \mathcal{S}_\star$)

$$\sum_{A\in\mathcal{V}_\sigma} u_A N_{A\sigma}^K = 0 \;\Leftrightarrow\; \exists b\in\mathbb{R},\; u_A = b\ (\forall A\in\mathcal{V}_\sigma).$$

As a matter of fact, $\mathrm{vect}(N_{A\sigma};\ A\in\mathcal{V}_\sigma)$ is exactly $(x_\sigma - x_K)^\perp$, the hyperplane perpendicular to $x_\sigma - x_K$ (this is easy to check). Consequently, we have $\mathbb{R}^d = N_{K\sigma}\oplus \mathrm{vect}(N_{A\sigma};\ A\in\mathcal{V}_\sigma)$; otherwise, $N_{K\sigma}\in(x_\sigma - x_K)^\perp$, meaning that $(x_\sigma - x_K)$ is parallel to σ, which is impossible. As a result

$$\mathbf{p}_{K\sigma} = 0 \Leftrightarrow u_K = u_\sigma,\ \exists b\in\mathbb{R},\ u_A = b\ (\forall A\in\mathcal{V}_\sigma).$$

The global result holds because, for any distinct K_1 and K_2 in $\mathcal{T}$, we can find a finite sequence of $(K_i,\sigma_i)_{i=1\dots P}$ $(\sigma_i\in\delta K_i)$ such that $|u_{K_1}-u_{K_2}|\le\sum_i|u_{K_i}-u_{\sigma_i}|$, see [10]; and similarly, for any $A_1\neq A_2$ in $\mathcal{V}$, we can find a finite sequence $(\sigma_j,A_j,B_j)_{j=1\dots Q}$ $(A_j,B_j\in\mathcal{V}_{\sigma_j})$ such that $u_{A_1}-u_{A_2}=\sum_j(u_{A_j}-u_{B_j})$. □

Remark 4.1. *If an homogeneous Neumann boundary condition is set on $\Gamma=\partial\Omega$, then the solution of $\mathbf{p}_{K\sigma}=0$ is given by two constant functions, $u_K=u_\sigma=a$ and $u_A=b$; while, if a Dirichlet boundary condition is set on a subset of Γ, then there exists at least one edge $\sigma\in\delta\mathcal{S}^1$ (the Dirichlet boundary) and then one vertex $A\in\mathcal{V}_\sigma\subset\mathcal{V}^1$ such that $u_A=u_\sigma=0$; and then the solution is $u_K=u_\sigma=u_A=0$.*

Now, given $\mathbf{u}\in FV(\Omega)$, and G having left and right limit values $G_{K\sigma}$ and $G_{L\sigma}$ on each $\sigma\in\mathcal{S}$, we can define some fluxes for $K\in\mathcal{T}$ and $\sigma\in\delta K$, and $A\in\mathcal{V}_\sigma$[3],

$$F_{K\sigma} = G_{K\sigma}p_{K\sigma}(\mathbf{u})\cdot N_{K\sigma},$$

$$F_{A\sigma} = \begin{cases} G_{K\sigma}p_{K\sigma}(\mathbf{u})\cdot N_{A\sigma}^K + G_{L\sigma}p_{L\sigma}(\mathbf{u})\cdot N_{A\sigma}^L & \text{if } \sigma = K\cap L\in\mathcal{S}_\star,\\ G_{K\sigma}p_{K\sigma}(\mathbf{u})\cdot\left(N_{A\sigma}^K + \frac{d-1}{d}N_{K\sigma}\right) & \text{if } \sigma\in\delta\mathcal{S}, \end{cases}$$

so that

$$\left(\sum_{\sigma\in\delta K}F_{K\sigma},\ \sum_{\sigma\in\mathcal{S}_A}F_{A\sigma}\right)_{K\in\mathcal{T},A\in\mathcal{V}\setminus\mathcal{V}^1}$$

[3]the u_σ are given by the conservativity relation (41)

are discretizations of $\int_K \operatorname{div}(G\nabla u)$ on the cells K and $\int_{D(A)} \operatorname{div}(G\nabla u)$ on the the V-cells $D(A)$.

Theorem 4.1 (Discrete Green Formula)**.** *Given* $\mathbf{u}, \mathbf{v} \in FV(\Omega)$*, we have*

$$
\begin{aligned}
&- \sum_{K\in\mathcal{T}} v_K \left(\sum_{\sigma\in\delta K} F_{K\sigma} \right) - \sum_{A\in\mathcal{V}} v_A \left(\sum_{\sigma\in\mathcal{S}_A} F_{A\sigma} \right) \\
&\qquad = d \sum_{\sigma\in\mathcal{S}_\star} \left(G_{K\sigma}\mathbf{p}_{K\sigma}(\mathbf{u}) \cdot \mathbf{p}_{K\sigma}(\mathbf{v}) + G_{L\sigma}\mathbf{p}_{L\sigma}(\mathbf{u}) \cdot \mathbf{p}_{L\sigma}(\mathbf{v}) \right) \\
&\quad + d \sum_{\sigma\in\delta\mathcal{S}} G_{K\sigma}\mathbf{p}_{K\sigma}(\mathbf{u}) \cdot \mathbf{p}_{K\sigma}(\mathbf{v}) - d \sum_{\sigma\in\delta\mathcal{S}} \gamma_{K\sigma}(\mathbf{v}) G_{K\sigma}\mathbf{p}_{K\sigma}(\mathbf{u}) \cdot N_{K\sigma},
\end{aligned}
$$

where the trace $\gamma_{K\sigma}(\mathbf{v})$ *on* $\sigma \in \delta\mathcal{S}$ *(such that* $\sigma \in \delta K$*) is given by*

$$
\gamma_{K\sigma}(\mathbf{v}) = \frac{1}{d} \left(v_\sigma + (d-1) \sum_{A\in\mathcal{V}_\sigma} \frac{v_A}{d} \right). \tag{46}
$$

Proof. The proof proceeds in three steps : rewriting the sums into sums on the edges $\sigma \in \mathcal{S}$, splitting into the interior ($\sigma \in \mathcal{S}_\star$) and a boundary ($\sigma \in \delta\mathcal{S}$) parts, and finally identifying the $\mathbf{p}_{K\sigma}(\mathbf{v})$, $\mathbf{p}_{L\sigma}(\mathbf{v})$ in the result:

$$
\begin{aligned}
& - \sum_{K\in\mathcal{T}} v_K \left(\sum_{\sigma\in\delta K} F_{K\sigma} \right) - \sum_{A\in\mathcal{V}} v_A \left(\sum_{\sigma\in\mathcal{S}_A} F_{A\sigma} \right) \\
= \; & - \sum_{\sigma\in\mathcal{S}_\star} \left(G_{K\sigma}\mathbf{p}_{K\sigma}(\mathbf{u}) \cdot v_K N_{K\sigma} + G_{L\sigma}\mathbf{p}_{L\sigma}(\mathbf{u}) \cdot v_L N_{L\sigma} \right) \\
& - \sum_{\sigma\in\mathcal{S}_\star} \sum_{A\in\mathcal{V}_\sigma} \left(G_{K\sigma}\mathbf{p}_{K\sigma}(\mathbf{u}) \cdot v_A N^K_{A\sigma} + G_{L\sigma}\mathbf{p}_{L\sigma}(\mathbf{u}) \cdot v_A N^L_{A\sigma} \right) \\
& - \sum_{\sigma\in\delta\mathcal{S}} G_{K\sigma}\mathbf{p}_{K\sigma}(\mathbf{u}) \cdot v_K N_{K\sigma} \\
& - \sum_{\sigma\in\delta\mathcal{S}} \sum_{A\in\mathcal{V}_\sigma} G_{K\sigma}\mathbf{p}_{K\sigma}(\mathbf{u}) \cdot v_A \left(N^K_{A\sigma} + \frac{d-1}{d} N_{K\sigma} \right) \\
= \; & \sum_{\sigma\in\mathcal{S}_\star} \left(d|D_K(\sigma)| G_{K\sigma}\mathbf{p}_{K\sigma}(\mathbf{u}) \cdot \mathbf{p}_{K\sigma}(\mathbf{v}) \right. \\
& \qquad \left. + d|D_L(\sigma)| G_{L\sigma}\mathbf{p}_{L\sigma}(\mathbf{u}) \cdot \mathbf{p}_{L\sigma}(\mathbf{v}) \right) \\
& + \sum_{\sigma\in\delta\mathcal{S}} d|D_K(\sigma)| G_{K\sigma}\mathbf{p}_{K\sigma}(\mathbf{u}) \cdot \mathbf{p}_{K\sigma}(\mathbf{v}) \\
& - \sum_{\sigma\in\delta\mathcal{S}} G_{K\sigma}\mathbf{p}_{K\sigma}(\mathbf{u}) \cdot \left(v_\sigma N_{K\sigma} + \sum_{A\in\mathcal{V}_\sigma} v_A \frac{d-1}{d} N_{K\sigma} \right).
\end{aligned}
$$

□

Theorem 4.2 (Corollary)**.** *Now if we set an homogeneous Dirichlet - Neumann boundary condition $u_\sigma = 0$, $u_A = 0$ for $\sigma \in \delta\mathcal{S}^1$ and $A \in \mathcal{V}_\sigma$; and $G_{K\sigma}\mathbf{p}_{K\sigma}(\mathbf{u}) \cdot N_{K\sigma} = 0$ for $\sigma \in \delta\mathcal{S}^2$, then the bilinear operator*

$$Q_{\mathcal{M}}(\mathbf{u}, \mathbf{v}) = -\sum_{K\in\mathcal{T}} v_K \left(\sum_{\sigma\in\delta K} F_{K\sigma} \right) - \sum_{A\in\mathcal{V}} v_A \left(\sum_{\sigma\in\mathcal{S}_A} F_{A\sigma} \right)$$

is Symmetric and Positive-Definite on the space $FV(\Omega)$ of functions $\mathbf{v} = (v_K, v_A)$ such that $v_\sigma = 0$, $v_A = 0$ for $\sigma \in \delta\mathcal{S}^1$ and $A \in \mathcal{V}_\sigma$.

Proof. In this case, either $G_{K\sigma}\mathbf{p}_{K\sigma}(\mathbf{u})\cdot N_{K\sigma} = 0$ if $\sigma \in \delta\mathcal{S}^2$, or $\gamma_{K\sigma}(\mathbf{v}) = 0$ if $\sigma \in \delta\mathcal{S}^1$, so that

$$Q_{\mathcal{M}}(\mathbf{u}, \mathbf{v}) = d \sum_{\sigma\in\mathcal{S}_\star} \left(G_{K\sigma}\mathbf{p}_{K\sigma}(\mathbf{u}) \cdot \mathbf{p}_{K\sigma}(\mathbf{v}) + G_{L\sigma}\mathbf{p}_{L\sigma}(\mathbf{u}) \cdot \mathbf{p}_{L\sigma}(\mathbf{v}) \right) + d \sum_{\sigma\in\delta\mathcal{S}} G_{K\sigma}\mathbf{p}_{K\sigma}(\mathbf{u}) \cdot \mathbf{p}_{K\sigma}(\mathbf{v})$$

is Symmetric and Positive. At last, if $Q(\mathbf{u}, \mathbf{u}) = 0$, then $\mathbf{p}_{K\sigma}(\mathbf{u}) = 0$ for all $K \in \mathcal{T}$ and $\sigma \in \delta K$, so that $\mathbf{u} = 0$, due to proposition 4.4 and remark 4.1. □

4.6. **Expression of the Fluxes for the Bidomain Problem.** The fluxes F^e are defined inside H only: if $\sigma = K \cap L \in \mathcal{S}_H$, then (for any $A \in \mathcal{V}_\sigma$)

$$F^e_{K\sigma} = -F^e_{L\sigma} = G_{e\sigma}\mathbf{p}_\sigma(\mathbf{v}) \cdot N_{K\sigma}, \tag{47}$$

$$F^e_{A\sigma} = G_{e\sigma}\mathbf{p}_\sigma(\mathbf{v}) \cdot N_{A\sigma}; \tag{48}$$

if $\sigma = K \cap L \in \mathcal{S}_\Sigma$ and $K \in \mathcal{T}_H$, then (for any $A \in \mathcal{V}_\sigma$)

$$F^e_{K\sigma} = G_{e\sigma}\mathbf{p}_{K\sigma}(\mathbf{v}) \cdot N_{K\sigma}, \tag{49}$$

$$F^e_{A\sigma} = G_{e\sigma}\mathbf{p}_{K\sigma}(\mathbf{v}) \cdot \left(N^K_{A\sigma} + \frac{d-1}{d} N_{K\sigma} \right) \tag{50}$$

(see (35)).

The fluxes F are defined inside Ω: if $\sigma = K \cap L \in S_H$, then (for any $A \in \mathcal{V}_\sigma$)

$$F_{K\sigma} = -F_{L\sigma} = (G_{i\sigma} + G_{e\sigma})\mathbf{p}_\sigma(\mathbf{v}) \cdot N_{K\sigma}, \tag{51}$$

$$F_{A\sigma} = (G_{i\sigma} + G_{e\sigma})\mathbf{p}_\sigma(\mathbf{v}) \cdot N_{A\sigma}; \tag{52}$$

if $\sigma = K \cap L \in \mathcal{S}_\Sigma$ and $K \in \mathcal{T}_H$, $L \in \mathcal{T}_T$, then (for any $A \in \mathcal{V}_\sigma$)

$$F_{K\sigma} = -F_{L\sigma} = G_{e\sigma}\mathbf{p}_{K\sigma}(\mathbf{v}) \cdot N_{K\sigma} = -G_{T\sigma}\mathbf{p}_{L\sigma}(\mathbf{v}) \cdot N_{L\sigma}, \tag{53}$$

$$F_{A\sigma} = G_{e\sigma}\mathbf{p}_{K\sigma}(\mathbf{v}) \cdot N^K_{A\sigma} + G_{T\sigma}\mathbf{p}_{L\sigma}(\mathbf{v}) \cdot N^L_{A\sigma}; \tag{54}$$

if $\sigma = K \cap L \in S_T$, then (for any $A \in \mathcal{V}_\sigma$)

$$F_{K\sigma} = -F_{L\sigma} = G_{T\sigma}\mathbf{p}_\sigma(\mathbf{v}) \cdot N_{K\sigma}, \tag{55}$$

$$F_{A\sigma} = G_{T\sigma}\mathbf{p}_\sigma(\mathbf{v}) \cdot N_{A\sigma}; \tag{56}$$

if $\sigma = \delta\mathcal{S}$ and $\sigma \in \delta K$ ($K \in \mathcal{T}_T$), then (for any $A \in \mathcal{V}_\sigma$)

$$F_{K\sigma} = G_{T\sigma}\mathbf{p}_{K\sigma}(\mathbf{v}) \cdot N_{K\sigma}, \tag{57}$$

$$F_{A\sigma} = G_{T\sigma}\mathbf{p}_{K\sigma}(\mathbf{v}) \cdot \left(N_{A\sigma} + \frac{d-1}{d} N_{K\sigma} \right). \tag{58}$$

And at last, the fluxes F^i are defined inside Ω: if $\sigma = K \cap L \in S_H$, then (for any $A \in \mathcal{V}_\sigma$)

$$F^i_{K\sigma} = -F^i_{L\sigma} = G_{i\sigma}\mathbf{p}_\sigma(\mathbf{u}) \cdot N_{K\sigma}, \tag{59}$$

$$F^i_{A\sigma} = G_{i\sigma}\mathbf{p}_\sigma(\mathbf{u}) \cdot N_{A\sigma}; \tag{60}$$

if $\sigma = K \cap L \in \mathcal{S}_\Sigma$ and $K \in \mathcal{T}_H$, $L \in \mathcal{T}_T$, then (for any $A \in \mathcal{V}_\sigma$)

$$F^i_{K\sigma} = -F^i_{L\sigma} = 0, \tag{61}$$

$$F^i_{A\sigma} = G_{i\sigma}\mathbf{p}_{K\sigma}(\mathbf{u}) \cdot N^K_{A\sigma}; \tag{62}$$

if $\sigma \in S_T \cup \delta\mathcal{S}$, then (for any $A \in \mathcal{V}_\sigma$)

$$F^i_{K\sigma} = -F^i_{L\sigma} = 0, \tag{63}$$

$$F^i_{A\sigma} = 0. \tag{64}$$

5. Resolution of the bidomain equations

5.1. **Well-posedness of the discrete space problem.** Two spaces $FV(H)$ and $FV(\Omega)$ accounting for the boundary conditions (7) are given; and the fluxes F^e, F and F^i defined by (47)-(64) provide three bilinear operators,

$$Q_e(\mathbf{v}, \mathbf{u}') = -\sum_{K \in \mathcal{T}_H} u'_K \left(\sum_{\sigma \in \delta K} F^e_{K\sigma} \right) - \sum_{A \in \mathcal{V}_H \cup \mathcal{V}_\Sigma} u'_A \left(\sum_{\sigma \in \mathcal{S}_A} F^e_{A\sigma} \right)$$

$$Q(\mathbf{v}, \mathbf{v}') = -\sum_{K \in \mathcal{T}} v'_K \left(\sum_{\sigma \in \delta K} F_{K\sigma} \right) - \sum_{A \in \mathcal{V}} v'_A \left(\sum_{\sigma \in \mathcal{S}_A} F_{A\sigma} \right)$$

$$Q_i(\mathbf{u}, \mathbf{v}') = -\sum_{K \in \mathcal{T}} v'_K \left(\sum_{\sigma \in \delta K} F^i_{K\sigma} \right) - \sum_{A \in \mathcal{V}} v'_A \left(\sum_{\sigma \in \mathcal{S}_A} F^i_{A\sigma} \right),$$

defined respectively on $FV(\Omega)\times FV(H)$, $FV(\Omega)\times FV(\Omega)$, $FV(H)\times FV(\Omega)$. By convention, $\mathbf{u},\mathbf{u}'\in FV(H)$ and $\mathbf{v},\mathbf{v}'\in FV(\Omega)$.

Note that u_K, u_A are average values, and the correct finite volume formulation is based on the averages of (16) and (20), so that the equations must be divided by $|K|$ and $|D(A)|$ appropriately. Hence, consider the diagonal matrices

$$B_H = \operatorname{diag}\left(|K|,|H\cap D(A)|\right)_{K\in\mathcal{T}_H,\,A\in\mathcal{V}_H\cup\mathcal{V}_\Sigma},$$
$$B = \operatorname{diag}\left(|K|,|D(A)|\right)_{K\in\mathcal{T},\,A\in\mathcal{V}\setminus\mathcal{V}_1},$$

and $\hat{A}_e$, $\hat{A}$, $\hat{A}_i$ the matrices of Q_e, Q, Q_i. Then the finite volume method writes

$$A_mC_m\left(\mathbf{u}'(t)+I_{ion}\right) = -A_e\mathbf{v}(t), \tag{65}$$
$$A\mathbf{v}(t) = -A_i\mathbf{u}(t), \tag{66}$$

with

$$A_e = B_H^{-1}\hat{A}_e,\quad A = B^{-1}\hat{A},\quad A_i = B^{-1}\hat{A}_i.$$

Focusing on the quasi-static problem of finding the extracellular and extracardiac potential fields $v=(u_e,u_T)$ for a given membrane potential field u, the following theorem is proved.

Theorem 5.1. *Given $\mathbf{u}\in FV(H)$, the quasi-static problem* (66) *or equivalently*

$$\hat{A}\mathbf{v} = -\hat{A}_i\mathbf{u},\quad \mathbf{v}\in FV(\Omega)$$

has a unique solution (in fact the latter version is symmetric and positive-definite).

Proof. The matrix $\hat{A}$ is the matrix of $Q(\mathbf{v},\mathbf{v}')$, defined like in section 4.5 for $\mathbf{v}$ and $\mathbf{v}'$ in $FV(\Omega)$ and $G_{K\sigma}=G_{i\sigma}+G_{e\sigma}$ if $K\in\mathcal{T}_H$ and $\sigma\in\delta K$ and $\sigma\notin\mathcal{S}_\Sigma$; $G_{K\sigma}=G_{e\sigma}$ if $K\in\mathcal{T}_H$ and $\sigma\in\delta K\cap\mathcal{S}_\Sigma$; and $G_{K\sigma}=G_{T\sigma}$ if $K\in\mathcal{T}_T$ and $\sigma\in\delta K$.

Since $\mathbf{p}_{K\sigma}(\mathbf{v})$ verifies the homogeneous Neumann boundary condition on $\delta\mathcal{S}^2$ and $FV(\Omega)$ account for the homogeneous Dirichlet boundary condition on $\delta\mathcal{S}^1$, the theorem 4.2 applies immediately. □

5.2. **Practical Implementation.** An explicit time-stepping method is used to solve (65), (66) with a time-step $\Delta t>0$:

$$A_mC_m\left(\frac{\mathbf{u}^{n+1}-\mathbf{u}^n}{\Delta t}+I_{ion}^n\right) = -A_e\mathbf{v}^n\quad(n\geq 0), \tag{67}$$
$$A\mathbf{v}^n = -A_i\mathbf{u}^n\quad(n\geq 0), \tag{68}$$

where $\mathbf{u}^0=(u_K^0,u_A^0)$ and we choose

$$\forall K\in\mathcal{T}_H,\ u_K^0 = u^0(x_K),\quad \forall A\in\mathcal{V}_H\cup\mathcal{V}_\Sigma,\ u_A^0 = u^0(x_A).$$

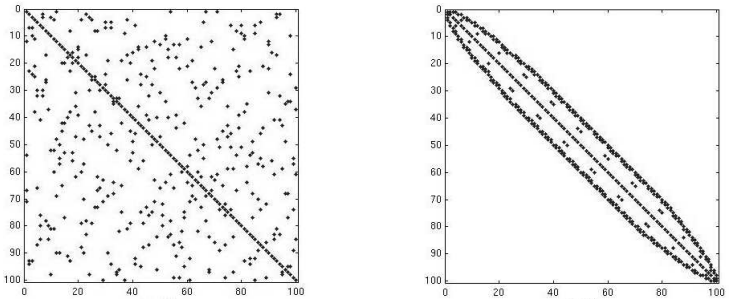

FIGURE 5. SRCM renumbering

At time $t^n = n\Delta t$ ($n \geq 0$), we successively

- solve the linear system (68) in order to find $\mathbf{v}^n$;
- do all the computations concerning the ionic current I_{ion}^n;
- update the transmembrane potential, ie compute $\mathbf{u}^{n+1}$.

The last point is straightforward, once the first two ones are correctly achieved.

Linear system. Its size is $N_{\mathcal{T}} + N_{\mathcal{V}} - N_{\mathcal{V}}^1$ (the number of volumes and points – except the Dirichlet ones); and it has to be solved for each time step. The numerical method to handle it has to be wisely chosen. Two methods seem particularly appropriate:

(1) A bi-conjugate gradient algorithm, due to lack of symmetry in (68). In that case, the BICGStab improvement is used.
(2) A GMRes algorithm is also possible after symmetrizing (68). This symmetrization does only depend on the measures of our volumes and can simply be viewed as a preconditioner.

Moreover the anisotropies, mesh structures as well as the size of the problem cause the system to be very ill-conditioned most of the times. Hence a good choice of preconditioner can drastically improve the convergence.

First of all, the numbering in unstructured meshes is often terrible as neighbor elements may have very different numbers. Hence, the sparse matrix A may have a distorted profile (see figure 5 left). To cope with this, a first preconditioning matrix is constructed by renumbering with a symmetric reverse Cuthill-McKee (SRCM) algorithm (see figure 5 right). Once the cells and vertexes are reordered correctly, a simple incomplete LU algorithm makes a very good preconditioner. Therefore, our choice of preconditioning is to stack the SRCM and ILU(p) matrices -and the symmetrizer before GMRes-. Most of the times setting p to 0 or 1 is the most efficient choice since higher p require much more

operations and seldom reduce enough the number of iterations to be competitive.

Of course, the preconditioner has only to be built once for all. Thus the resulting method proves to be quite efficient in our purpose.

Ionic model. The computation of ionic current involves the treatment of gate variables and other processes (pumps, exchangers, buffers,...) most of them strongly dependent on at least one other variable (such as u). While it is obviously crucial to perform a relevant approximation, it is also essential to avoid excessive computational costs. The methods used to make this approximation depends on the variables.

The greatest care was taken to compute the gates involved in the fast Na^+ current both because of its critical importance for the depolarization process and because of its very fast dynamics. In fact, during this depolarization, *a fourth-order Runge-Kutta method* is used if the time step overcome a threshold value. Aside from that case, these gates are treated as the others since their impact is then clearly less important.

Most of the gates and concentrations where updated using either an *Euler method* or an *analytical formula* assuming that u is constant inside each time step. This assumption proves to be particularly appropriate in the re-polarization zones where u varies very slowly.

Finally, intracellular Ca^{2+} buffering is computed following the analytical formulation of Zeng et al [34] which assume a steady-state for the buffering reaction.

It is to note first of all that these computations are purely local. Therefore, they are very easy to parallelize. Moreover, profiled simulations have shown (see below) that even for the more sophisticated models involving dozens of variables, only a very small amount of CPU time is required to compute the ionic current compared to the resolution of the linear system. Indeed, choosing a more realistic model is not penalizing in terms of CPU time.

6. Numerical Simulations

6.1. **Monodomain.** The monodomain case is reached when $T = \emptyset$ (the heart is isolated) and $G_i(x) = \lambda G_e(x)$ for all $x \in H$ with a fixed λ. In that case, the unknowns u_T, u_e can be dropped and the problem reduces to

$$A_m C_m \left(\partial_t u + I_{ion}\right) = \frac{\lambda}{1+\lambda} \operatorname{div}(G_e \nabla u).$$

with homogeneous Neumann boundary conditions and an initial data $u(0,x) = u^0(x)$ $(x \in H)$. There is no more linear system to be solved.

Comparison of several Finite Volumes Schemes. This first simulation intends to compare the finite volumes scheme previously described to "classical" finite volume approach explained in [10].

In the 2D uncoupled monodomain case considered, H is a simple 1 cm-radius disk initially fully polarized. The conductivities are set to 1 in fiber's direction and 0.1 otherwise. At time $t = 10\ ms$, a stimulus is applied at the center of the disk generating an expected circular depolarization wave. The results below are given at $t = 20\ ms$. The reference solution is given by a computation on a very fine mesh (with 69780 elements). The mesh used to compare the solution has 2123 elements and a computation has also been carried on a refined mesh (with 4309 elements) so that the total number of unknowns of the classical approach is greater than its counterpart with the DDFV method.

Obviously, the result of the classical approach is not a good approximation of the reference solution. The predicted wave deforms with mesh directions and ends to be very slow. It is to note that this deformation is sometimes critical on very disturbed meshes. On the other hand, the prediction of the DDFV method proves to be good, having a good circular shape only modulated by the elements and a speed which is close enough to the reference's. This simple example emphasizes the importance of carefully choosing the numerical method and shows that the DDFV better accounts for anisotropy than the classical finite volume method.

The same computation has been completed on several levels of refinement to have an overview of the convergence process. Eight meshes where used, consisting in respectively 551, 1069, 2123, 4309, 8721, 17270, 34017 and 69780 (reference) unknowns (ie volumes+vertexes). The next figures shows the relative error of the method in logarithmic scale. Aside from the first point, the error has a characteristic linear shape which gives an order of 1.04.

6.2. **Bidomain ECG Computations.** In order to facilitate the comparisons, each of the following examples share the same geometry which mesh is shown in figure 8. A 8×6 cm elliptic heart with a ventricular cavity is placed inside a 15×8 cm torso. The mass potential is set near the middle of the northwest part of the border. The parameters where fixed to $A_m = 2000\ cm^{-1}$, $C_m = 1\ \mu F.cm^{-2}$ and the intracellular and extracellular conductivities where respectively set to 4 $mS.cm^{-1}$ and 2 $mS.cm^{-1}$ in the fibers' direction and to 1.8 $mS.cm^{-1}$ and 1.5 $mS.cm^{-1}$ otherwise. The conductivity is also set to 2.39 $mS.cm^{-1}$ inside the torso and Faber-Rudy's improvement

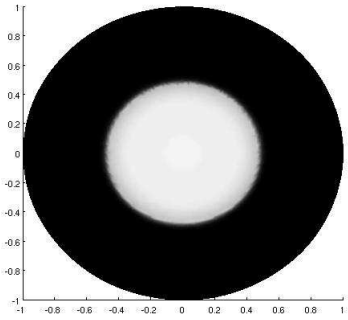

(a) Reference mesh of 69780 triangles)

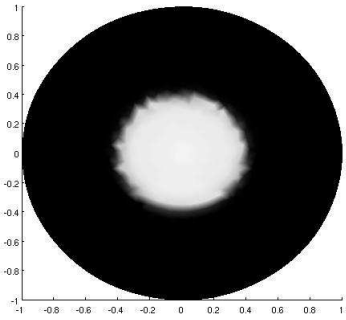

(b) DDFV Method with 2123 triangles

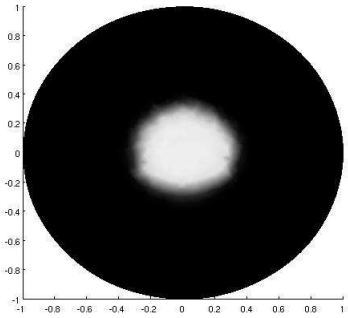

(c) Classical Method with 4309 triangles

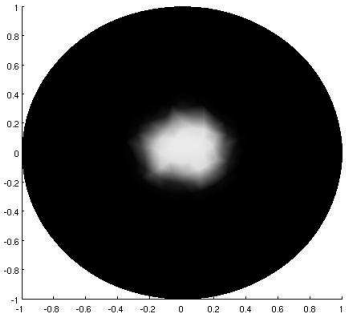

(d) Classical Method with 2123 triangles

FIGURE 6. Simulation of a Circular wave

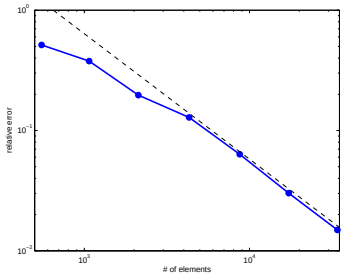

FIGURE 7. Convergence Rate of the Method

of Luo-Rudy II model is used for the computation of ionic currents. Finally, the stimulus are initiated on the axis at the left boundary between the heart and the ventricular cavity.

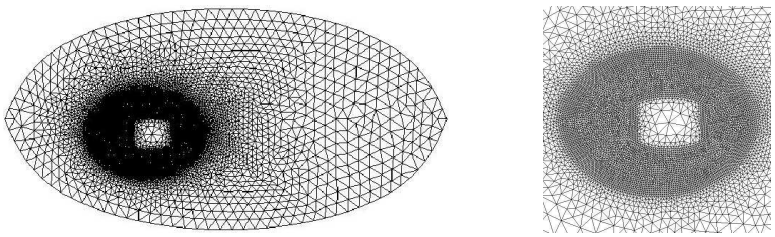

FIGURE 8. 2D mesh with 8854 triangles

Regular ECG, one Site of Stimulation. For this simulation, the electrical stimulus occurs at 100 bpm (hence once every 600 ms). This leads to the results shown on figure 9 and 10. The ECGs (figure 9, (a) to (d)) are extracted from 4 different points throughout the surface of the torso. The location of these electrodes is of course very important for the overall shape of the waves. Anyway, both QRS and T waves are easy to see and a regular beat can be observed.

The potential fields (figure 10) show the mechanisms of the evolution of v: since u_T does only depend on the values of u and u_e on the heart-torso interface Σ, it stays at rest until the wave reach this interface (left); and then (right) the whole torso is lit.

Regular ECG, two Sites of Stimulation. Now the same simulation is carried out with two stimuli initiated both on the left and the right of the ventricular cavity (figures 11 and 12). All of the ECGs of figure 11 are drawn using the same electrodes as before (figure 9. It is hence easy to see that the presence of this second source term has a huge impact on them, as expected. Once again anyway, both the QRS and T waves are visible and the beat is regular.

Profiling. On this simulation, the CPU time required by each part of the code has been profiled: for each time step, an average of 3.56% of the CPU time is spent for evaluating I_{ion} with Faber-Rudy's model [11] whereas 93.24% is spent for solving the linear system. Thus, even with a sophisticated ionic model, the time required for the computation of ionic process is not significant, which justifies the choice of realistic models compared to simplified ones.

Examples of irregular ECG. One of the edges of realistic models is the possibility to simulate various malfunctions. As an illustration, the results of *tachycardia* and *ischemia* are provided below.

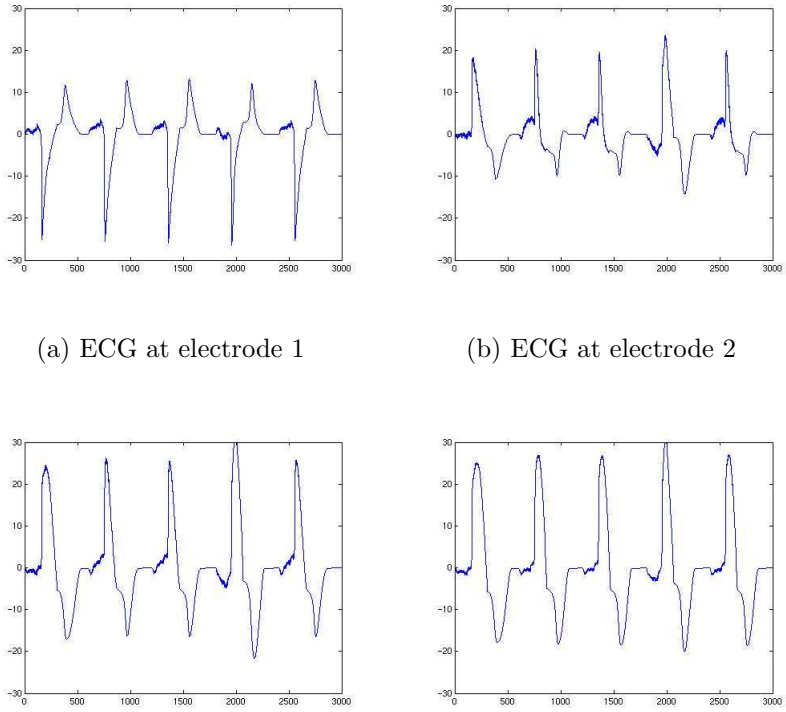

(a) ECG at electrode 1

(b) ECG at electrode 2

(c) ECG at electrode 3

(d) ECG at electrode 4

FIGURE 9. ECGs for a 1 site stimulus, 100bpm

Tachycardia results in a increase of the beat rate of the heart. Here, the stimulus is set to occur once every 250 ms (240 bpm) and the two-stimulus configuration introduced above is used. The results are shown in figure 13. There are several very interesting facts. First, after a transitional period, a regular beat appears which has no T wave. It is also worth noticing that the right stimulus does only play a role on the first beat. After, it always occurs in a zone where the Na u-dependent gates are closed and thus cannot have any effect (see the shape of u figure 13). At last the intracellular Calcium accumulates, whereas it resumes back to equilibrium for a regular beat, see figure 14.

Ischemia can also be simulated using Shaw and Rudy's improved Luo-Rudy II model ([30]). This disease is characterized by acidosis, anoxia and elevated concentration of extracellular potassium. The computed ECGs as shown in figure 15. There are modified as expected.

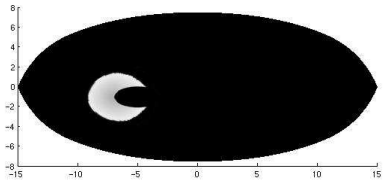

(a) Transmembrane potential u at $t = 140ms$

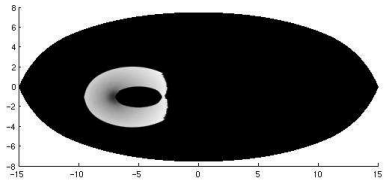

(b) Transmembrane potential u at $t = 240ms$

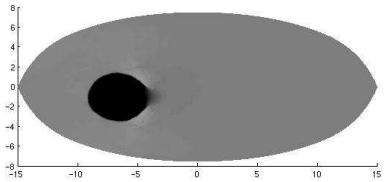

(c) Extracellular and Extracardiac potentials $v = (u_e, u_T)$ at $t = 140ms$

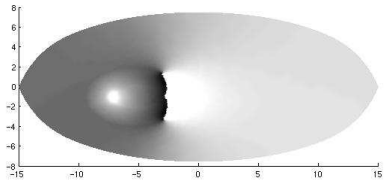

(d) Extracellular and Extracardiac potentials $v = (u_e, u_T)$ at $t = 240ms$

FIGURE 10. Potential Distributions (1 site stimulus)

A 3D Bidomain Compuation. 3D ECGs could not be computed yet, because adequate meshes are missing up to now. Indeed, a realistic simulation needs a very fine mesh of the 3D heart and the torso together with the data of the fibers directions in the heart. Hence, an anisotropic bidomain computation has been performed on a 3D mesh of a dog's heart considered isolated (see section 2.1). The mesh consists in 8363 volumes and 3763 vertexes, together with fibers directions. It has been previously constructed [29] upon the geometrical model from [26]. Faber-Rudy's improvement of Luo-Rudy II model has been used for the computation of ionic currents. The parameters of the previous 2D computations are used, except $A_m = 100$. The mesh is too coarse for larger values of A_m to be used (in that case, a *propagation failure* phenomena occurs). The results are shown in figure 16, where the regions at rest are in blue while the activated regions are in red. The first line of figure 16 shows the depolarization of the ventricles, and the second line its repolarization.

REFERENCES

[1] B Andreianov, F. Boyer, and F. Hubert. Discrete duality finite volume scheme for leray-lions type elliptic problems on general 2d meshes. *Submitted*, 2005.

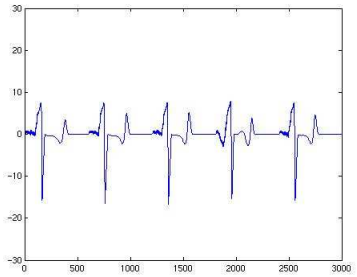

(a) ECG at electrode 1

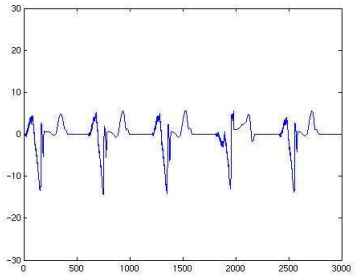

(b) ECG at electrode 2

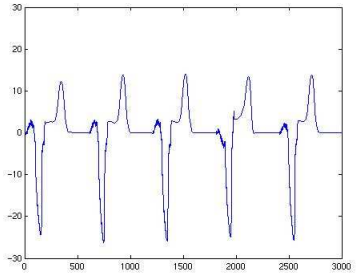

(c) ECG at electrode 3

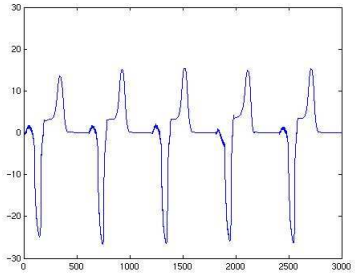

(d) ECG at electrode 4

FIGURE 11. ECGs for a 2 sites stimulus, 100bpm

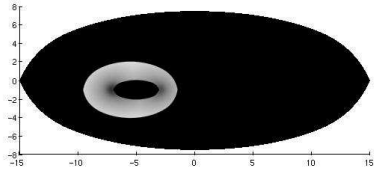

(a) Transmembrane potential u at $t = 240ms$

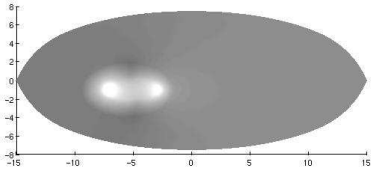

(b) Extracellular and Extracardiac potentials $v = (u_e, u_T)$ at $t = 240ms$

FIGURE 12. Potential Distributions (2 sites stimulus)

[2] G.W. Beeler and H. Reuter. Reconstruction of the Action Potential of Ventricular Myocardial Fibres. *J. Physiol.*, 268:177–210, 1977.

[3] J.-D. Boissonnat and M. Yvinec. *Algorithmic Geometry*. Cambridge University Press, 1998.

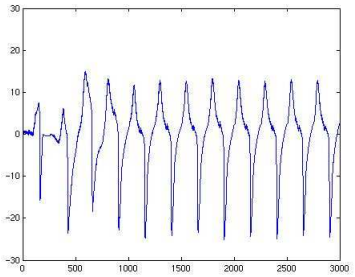

(a) ECG at electrode 1

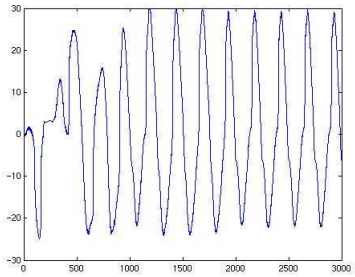

(b) ECG at electrode 2

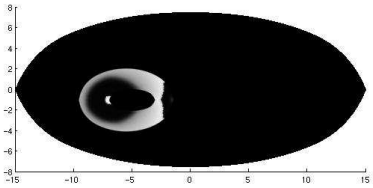

(c) Transmembrane Potential

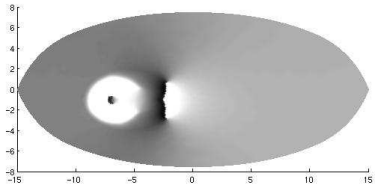

(d) Extracellular and Extracardiac potentials $v = (u_e, u_T)$

FIGURE 13. Tachycardia (240 bpm)

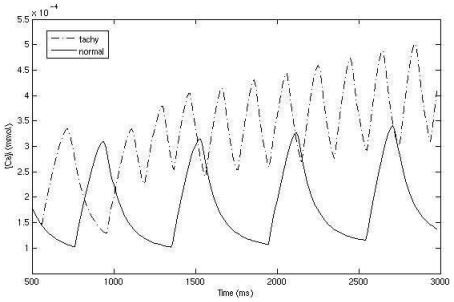

FIGURE 14. Intracellular Calcium in one point

[4] P. Colli Franzone, P. Deuflhard, B. Erdmann, J. Lang, and L.F. Pavarino. Adaptativity in space and time for reaction-diffusion systems in electrocardiology. Technical report, Konrad-Zuze-Zentrum für Informationstechnik Berlin, 2005.

[5] P. Colli-Franzone, L. Guerri, M. Pennacchio, and B. Taccardi. Anisotropic mechanism for multiphasic unipolar electrograms. Simulation studies and experimental recordings. *Ann. Biomed. Engrg.*, 28:1326–1342., 2000.

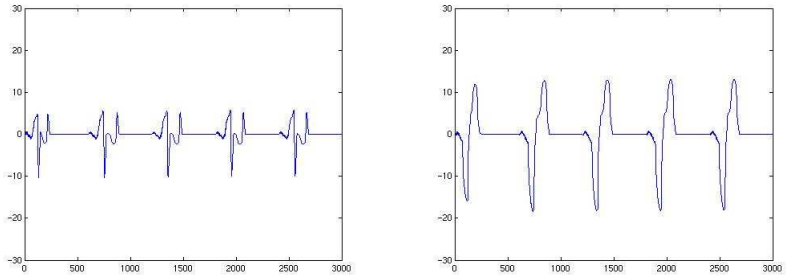

(a) ECG at electrode 1 (b) ECG at electrode 2

FIGURE 15. Ischemia

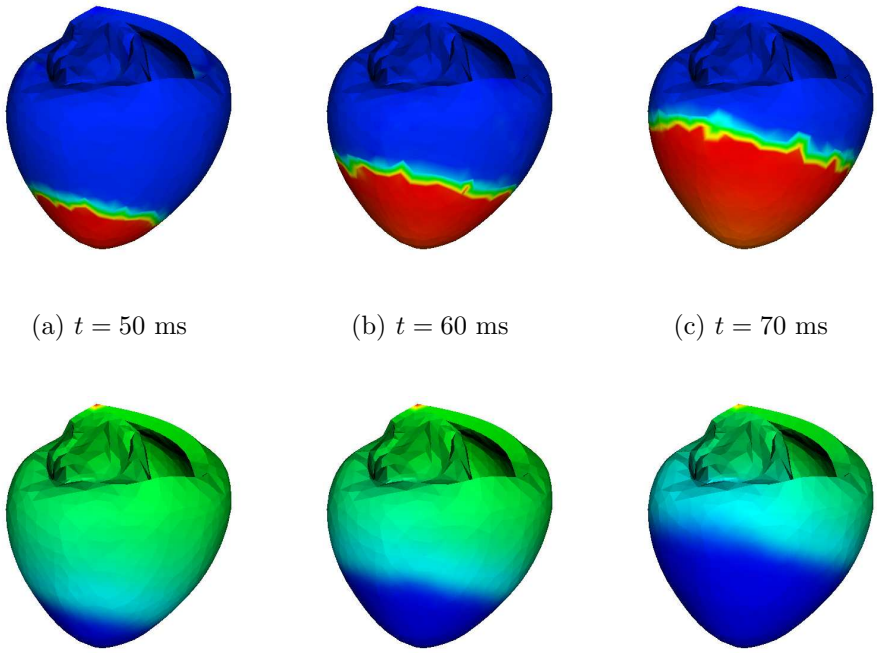

(a) $t = 50$ ms (b) $t = 60$ ms (c) $t = 70$ ms

(d) $t = 120$ ms (e) $t = 130$ ms (f) $t = 140$ ms

FIGURE 16. Example of a 3D Computation

[6] P. Colli-Franzone, L. Guerri, C. Viganotti, E. Macchi, S. Baruffi, S. Spaggiari, and B. Taccardi. Potential fields generated by oblique dipole layers modeling excitation wavefronts in the anisotropic myocardium. *Circ. Res.*, 51:330–346, 1982.

[7] P. Colli-Franzone and G. Savaré. Degenerate evolution systems modeling the cardiac electric field at micro- and macroscopic level. In Lorenzi, A and Ruf, B., editor, *Evolution equations, Semigroups and Functional Analysis*, pages 49–78. Birkhauser, 2002.

[8] Piero Colli-Franzone, Micol Pennacchio, and Luciano Guerri. Accurate computation of electrograms in the left ventricular wall. *Math. Models Methods Appl. Sci.*, 10(4):507–538, 2000.

[9] K. Domelevo and P. Omnes. A finite volume method for the Laplace operator on almost arbitrary two-dimensional grids. *M2AN*, to appear, 2005.

[10] R. Eymard, T. Gallouët, and R. Herbin. *Finite volume methods.* Ciarlet, P. G. (ed.) et al., Handbook of numerical analysis. Vol. 7, 2000.

[11] G. Faber and Y. Rudy. Action Potential and Contractility Changes in [Na+]i Overloaded Cardiac Myocytes: A Simulation Study. *Biophysical Journal*, 78:2392–2404, 2000.

[12] R. Fitzhugh. Impulses and physiological states in theoretical models of nerve membrane. *Biophys. J.*, 1:445–465, 1961.

[13] C.S. Henriquez. Simulating the electrical behaviour of cardiac tissue using the bidomain model. *Crit. Rev. Biomed. Engr.*, 21:1–77, 1993.

[14] F. Hermeline. A finite volume method for the approximation of diffusion operators on distorted meshes. *J. Comput. Phys.*, 160(2):481–499, 2000.

[15] F. Hermeline. Approximation of diffusion operators with discontinuous tensor coefficients on distorted meshes. *Comput. Methods Appl. Mech. Eng.*, 192(16-18):1939–1959, 2003.

[16] A.L. Hodgkin and A.F. Huxley. A quantitative description of membrane current and its application to conduction and excitation in nerve. *J. Physiol.*, 117:500–544, 1952.

[17] J.P. Keener and J. Sneyd. *Mathematical Physiology.* Springer-Verlag, 1998.

[18] W. Krassowska and J.C. Neu. Homogenization of syncytial tissues. *CRC Crit. Rev. Biomed. Eng.*, 21(2):137–199, 1993.

[19] W. Krassowska and J.C. Neu. Effective boundary conditions for syncytial tissues. *IEEE*, 41(2):143–150, 1994.

[20] G.L. Lines. *Simulating the Electrical Activity in the Heart - A Bidomain Model of the Ventrciles Embedded in a Torso* . Phd thesis, Department of informatics, University of Oslo,, 1999.

[21] G.T. Lines, P. Grottum, A.J. Pullan, J. Sundes, and A. Tveito. Mathematical models and numerical methods for the forward problem in cardiac electrophysiology. *Comput. Visual. Sci*, 5:215–239, 2003.

[22] G.T. Lines, P. Grottum, and A. Tveito. Modeling the electrical activity of the heart: a bidomain model of the ventricles embedded in a torso. *Comput. Viual. Sci.*, 5:195–213, 2003.

[23] C.H. Luo and Y. Rudy. A model of the Ventricular Cardiac Action Potential. *Circ. Res.*, 68:1501–1526, 1991.

[24] C.H. Luo and Y. Rudy. A Dynamic Model of the Cardiac Ventricular Action Potential. *Circ. Res.*, 74:1097–1113, 1994.

[25] C.H. Luo and Y. Rudy. A Dynamic Model of the Cardiac Ventricular Action Potential I. Simulations of Ionic Currents and Concentration Changes. *Circ. Res.*, 74:1071–1096, 1994.

[26] M. Nash. *Mechanics and Material Properties of the Heart using Anatomically Accurate Mathematical Model*. PhD thesis, University of Auckland, 1998.
[27] E. Page. Cat Heart Muscle in Vitro. Part III. The extracellular space . *J. Gen. Physio.*, 46:201–213, 1962.
[28] A. V. Panfilov and R. R Aliev. A simple two-variable model of cardiac excitation. *Chaos Solitons and Fractals*, 7(3):293–301, 1996.
[29] M. Sermesant, Y. Coudière, H. Delingette, N. Ayache, and J.A. Désidéri. An electro-mechanical model of the heart for cardiac image analysis. In W. J. Niessen and M. A. Viergever, editors, *Medical Image Computed and Computer-Assisted Intervention*, number 2208 in LNCS, pages 224–231, 2001.
[30] R.M. Shaw and Y. Rudy. Electrophysiologic Effects of Acute Myocardial Ischemia: a Theoretical Study of Altered Cell Excitability and Action Potential Duration. *Cardiovascular Research*, 35:256–272, 1997.
[31] K.H. Ten Tusscher, D. Noble, P.J. Noble, and A.V. Panfilov. A Model for Human Ventricular Tissue. *Am J Physiol Heart Circ Physiol*, 286, 2004.
[32] M. Trew, I. Le Grice, B.1 Smaill, and A. Pullan. A finite volume method for modeling discontinuous electrical activation in cardiac tissue. *Annals of Biomedical Engineering*, 33(5):590–602, 2005.
[33] A.D. Waller. A demonstration on man of electromotive changes accompanying the heart's beat. *J. Physiol.*, 8:229–234, 1887.
[34] J. Zeng, K.R. Laurita, D.S. Rosenbaum, and Y. Rudy. Two Components of the Delayed Rectifier K+ Current in Ventricular Myocytes of the Guinea Pig Type. *Circulation Research*, 77:140–152, 1995.